

1 **Contrasting ~~Inland-Coastal~~ Aerosol Mixing States at Inland and**
2 **Coastal Sites: An Entropy-Based Metric for CCN Activity**

3 Jingye Ren^{1,2}, Wei Xu³, Ru-Jin Huang^{1*}, Fang Zhang^{4*}, Ying Wang¹, Lu Chen⁵, Jurgita
4 Ovadnevaite⁶, Darius Ceburnis⁶, Colin O'Dowd⁶, Yele Sun⁷

5 ¹*State Key Laboratory of Loess Science, Institute of Earth Environment, Chinese*
6 *Academy of Sciences, Xi'an, 710061, China,*

7 ²*Xi'an Institute for Innovative Earth Environment Research, Xi'an, 710061, China,*

8 ³*State Key Laboratory of Advanced Environmental Technology, Institute of Urban*
9 *Environment, Chinese Academy of Sciences, Xiamen, 361021, China,*

10 ⁴*School of ~~Civil and Environmental Engineering~~Ecology and Environment, College of*
11 *Artificial Intelligence, Harbin Institute of Technology, Shenzhen, 518005, China,*

12 ⁵*School of Ocean and Geographic Science, Yancheng Teachers University, Yancheng*
13 *224051, China,*

14 ⁶*School of Natural Sciences, Centre for Climate & Air Pollution Studies, Ryan Institute,*
15 *University of Galway, University Road, Galway, Ireland.*

16 ⁷*State Key Laboratory of Atmospheric Boundary Layer Physics and Atmospheric*
17 *Chemistry, Institute of Atmospheric Physics, Chinese Academy of Sciences, Beijing*
18 *100029, China.*

19 Corresponding author: Ru-Jin Huang, *rujin.huang@ieecas.cn*; Fang Zhang,
20 *zhangfang2021@hit.edu.cn*

21

22

23

24

25

26

27 **Abstract**

28 Simplified assumptions of aerosol ~~hygroscopic~~ mixing states in modeling studies
29 often introduce substantial uncertainties in estimating cloud condensation nuclei (CCN)
30 concentrations (N_{CCN}) and their climatic impacts. This study systematically investigates
31 the contrasting relationships between mixing states and CCN activity by ~~comparing~~
32 ~~ambient~~ combining field measurements ~~from~~ of probability distribution function of the
33 hygroscopicity with the algorithm of entropy at two inland and coastal sites. We show
34 distinct seasonal variations of ~~the particles~~ aerosol mixing state. In winter, externally-
35 mixed particles dominated both sites, with comparable mixing state indices (χ) of
36 0.38 ± 0.12 and 0.39 ± 0.09 respectively for coastal air ~~masses~~ and inland air. However,
37 summer measurements showed pronounced differences: photochemical processes
38 promoted significantly higher internal mixing in coastal aerosols ($\chi = 0.69 \pm 0.19$),
39 whereas inland χ values only increased moderately to 0.47 ± 0.12 . Aerosol mixing state
40 is largely influenced by primary emissions and secondary formation process.
41 Externally-mixed particles originate chiefly from anthropogenic emissions in inland or
42 sea salt in coastal. During the aging process, particles become more internally-mixed
43 as the enhanced fraction of more-hygroscopic mode. A universal logarithmic
44 correlation was identified between the critical diameter (D_{cri}) characterizing CCN
45 activity and χ ($D_{cri} = -32.15 \ln(\chi) + 84.71$, Pearson $r = -0.74$), but with distinct decrement

46 rates for coastal vs. inland aerosols. ~~Our further quantitative~~Further analysis reveals a
47 0.1 increase in χ enhanced winter ~~CCN concentrations (N_{CCN})~~ by 39–65% ~~under typical~~
48 ~~cloud supersaturations, at the supersaturation of 0.2%~~, whereas this effect diminished to
49 ~9% in summer. These results underscore that mixing states exert ~~more~~
50 ~~pronounced~~different control over N_{CCN} in diverse environments. Our work provides
51 critical constraints for parameterizing fine aerosols CCN activity in climate models,
52 ~~thereby reducing uncertainties in aerosol–climate effect estimations.~~

53

54

55

56 **1. Introduction**

57 Atmospheric cloud condensation nuclei (CCNs) are complex mixtures of organic
58 and inorganic components. Their chemical and physical properties make quantifying
59 aerosol–cloud interactions challenging (Liu et al., 2018; Rosenfeld et al., 2019; Xu et
60 al., 2022, 2024; Virtanen et al., 2025), introducing uncertainties into climate effect
61 assessments (Charlson et al., 1992; Shrivastava et al., 2017; IPCC, 2021; [Chen et al.,](#)
62 [2022a](#); Manavi et al., 2025; ~~Chen et al., 2022~~). Accurate climate model predictions of
63 aerosol impacts require understanding aerosol mixing states under different
64 atmospheric conditions and their effects on CCN activity (Ching et al., 2016; Zheng et
65 al., ~~2021~~[2021a](#)). Current models often oversimplify mixing states by assuming pure
66 internal or external mixing (Winkler, 1973; ~~Zheng et al., 2021~~; Stevens et al., 2019;
67 Riemer et al., 2019); ~~Zheng et al., 2021b~~). This is problematic because mixing states

68 directly determine particle hygroscopicity distribution and CCN estimates (Wang et al.,
69 2010; ~~Ren~~Tao et al., ~~2018~~2024). For example, ~~CCN activity for internal-mixed aerosols~~
70 ~~rely more on inorganic components~~aerosol particles have unimodal hygroscopicity
71 distribution, while the external ~~mixtures~~mixed particles are ~~more sensitive to organic~~
72 ~~matter~~ (~~Ren~~characterized by the bimodal/trimodal or partly overlapping structures
73 (Spitieri et al., ~~2018~~2018; ~~Bhatta~~2023; Liu et al., ~~2015~~2025). Such simplifications can lead
74 to significant errors, e.g., Sotiropoulou et al. (2007) found that mixing state assumptions
75 caused two-fold N_{CCN} estimation errors in global models.

76 Systematic observations across diverse environments are critical because aerosol
77 mixing states exhibit pronounced spatial-temporal variations (Ye et al., 2018; ~~Liu et al.,~~
78 ~~2025~~; Hughes et al., 2018; Liu et al., 2025). For example, continental and coastal
79 regions present contrasting scenarios (Ramachandran et al., 2016). The continental
80 areas are dominated by anthropogenic emissions, where aerosol aging is driven by
81 industrial and traffic-related pollutants (Huang et al., 2014; Ren et al., 2023). Particles
82 here undergo progressive internal mixing via photochemical process and heterogenous
83 ~~reactions~~and coagulation, altering their hygroscopic properties (Ervens et al., 2010;
84 Tao et al., 2021). While the coastal regions feature dynamic interactions between
85 marine aerosols (e.g., sea salt) and continental pollutants (Schill et al., 2015; Collins et
86 al., 2013; Cheung et al., 2020). Seasonal shifts in air mass sources (e.g., marine vs.
87 continental dominance) might create unique mixing state patterns (Xu et al., 2020,
88 2021a). For instance, summer photochemical aging and heterogenous processes in
89 coastal areas can enhance the degree of internal mixing, while winter often retains more

90 external mixing due to ~~stable atmospheric conditions~~ the presence of the sea-salt
91 particles with less-hygroscopic organic matter.

92 ~~However, the aerosols in continental and coastal regions have distinct climate~~
93 ~~feedback mechanisms (Bellouin et al., 2019; Pan et al., 2022; Gong et al., 2023).~~ The
94 continental aerosols influence regional cloud formation, while coastal aerosols ~~affect~~
95 may provide insights into the characteristics of marine boundary layer clouds
96 ~~that~~ aerosols in region. The properties of marine aerosols are key components of global
97 ~~climate systems (significantly different from those of continental aerosols, and~~
98 ~~therefore have distinct climate feedback mechanisms (Bellouin et al., 2020; Xu et al.,~~
99 ~~2024; Liu et al., 2018).~~ But2024). However, the current models lack regional-specific
100 mixing state parameters and usually assume uniform mixing in both environments. This
101 could lead to large uncertainties in predicting CCN concentrations, highlighting the
102 need for site-specific observations. For example, Ren et al. (2018) found that the impact
103 of aerosol mixing state on CCN activation characteristics ranged from -34% to +16 %
104 in urban atmosphere. Comparison between a fully internal mixture assumption and
105 using the mixing state index from the particle-resolved model, Ching et al. (2017) found
106 the obvious overestimation in CCN concentration estimation. Especially in the regions
107 eg., Amazon Basin, Central Africa and Indonesia, the particles appeared to be more
108 external, errors in CCN concentration would increase up to 100% (Hughes et al., 2018).
109 A detailed exploration of mixing state on CCN concentration in global scale was
110 conducted by Zheng et al. (2021a), and the results showed that the mixing state varied
111 spatially with more externally mixed over the North Atlantic Ocean, off the coasts of

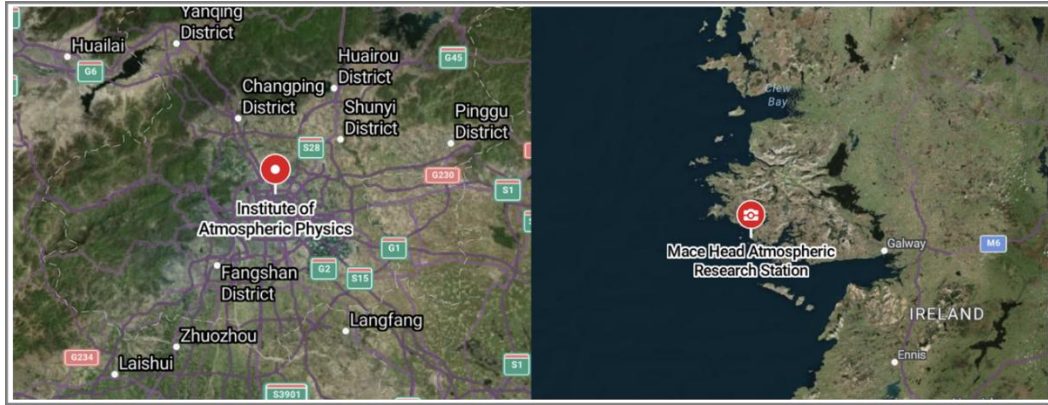
112 Southern Africa, and Australia. Thus, assuming particles with internally-mixed would
113 introduce errors in CCN concentration of 50-100%.

114 ~~Recent studies have used the mixing state index (χ) to characterize aerosol~~
115 ~~heterogeneity (Zheng et al., 2021; Ching et al., 2017; Yuan et al., 2023), but cross-~~
116 ~~environment comparisons remain limited. Therefore, for quantifying the aerosol mixing~~
117 state in the ambient atmosphere, we apply the algorithm of entropy proposed by Riemer
118 and West (2013) to investigate the aerosol heterogeneity. This index has been applied
119 to quantify the mixing state more reasonably both in field campaigns (Zhao et al., 2021;
120 Yuan et al., 2023) and model simulations (Ching et al., 2016; Zheng et al., 2021a).
121 However, most studies focused on quantifying the particle heterogeneity in composition
122 (Ching et al., 2019; Fierce et al., 2020; Zhao et al., 2021). Here we concentrated on
123 evaluating the heterogeneity in aerosol hygroscopicity for sub-micron particles, which
124 directly related to CCN budget. By refereeing to Yuan et al. 2023, the heterogeneity in
125 hygroscopicity was investigated by combining in-situ measurements of probability
126 distribution function of the hygroscopicity with the algorithm of entropy. Briefly, the
127 mixing state index χ , is devised based on the concept of information entropy concerning
128 the distribution of hygroscopicity across the aerosol population. It varies between 0
129 (external mixing completely) and 1 (internal mixing completely). By integrating inland
130 and coastal measurements, this study will focus on addressing two key gaps, (1) How
131 continental vs. marine-dominated environments shape aerosol mixing states and CCN
132 activity; (2) Whether χ -based CCN parameterizations show regional dependencies,
133 providing critical constraints for climate models.

134 2. Data and Methods

135 2.1 Field Campaigns

136 The inland atmospheric measurements were conducted for two ~~periods~~campaigns
137 from 16 November to 6 December 2016 and 29 May to 13 June, ~~respectively in urban~~
138 ~~Beijing, 2017 as a part of the Air Pollution and Human Health (APHH) project (Shi et~~
139 ~~al., 2019).~~ at the Institute of Atmospheric Physics, Chinese Academy of Sciences (IAP,
140 39.97° N, 116.37° E) in urban Beijing. The campaigns were complemented by the
141 hygroscopicity and CCN observations and were conducive to provide information on
142 the aerosol hygroscopicity affecting urban pollutions. This urban site exhibited highly
143 variable aerosol populations dominated by local anthropogenic sources including
144 vehicular, cooking emissions, and residential heating. Coastal measurements were
145 performed at the Mace Head atmospheric research station (MHD, 53.33° N, 9.90° W)
146 from 1 November 2009 to 30 January 2010, and summer periods from 11 to 31 August
147 2009 and July 2010, which located on the west coast of Ireland. Aerosol particles here
148 experience alternating influences from polluted continental and clean marine
149 atmospheres. The map of the sites was shown in Figure 1. More details about the
150 campaigns were given in Fan et al. (2020) and Xu et al. (2021a).



151
152 **Fig 1.** Map of the sites in the Inland of the Institute of Atmospheric Physics (IAP) and
153 Coastal of Mace Head (MHD). (© Google Maps, <https://maps.google.com/>, last access:
154 2 April 2025).

155 **2.2 Instrumentation**

156 **Hygroscopicity measurements**

157 The particle hygroscopicity at both sites was characterized using the humidified
158 tandem differential mobility analyzer (HTDMA). The hygroscopic growth factor (Gf),
159 defined as the ratio of the particle diameter at the fixed RH (90%) and dry diameter set
160 in this study for 40, 80, 110, 150, 200 nm at IAP and 35, 50, 75, 110 and 165 nm at
161 MHD, respectively. The Gf probability density function (Gf-PDF) was derived using
162 the TDMAinv algorithm (Gysel et al., 2009). The number fraction (NF) of near-
163 hydrophobic mode (NH: $Gf \leq 1.21$), and more hygroscopic mode (MH: $Gf > 1.21$) in
164 IAP site was referred from Chen et al. (2022b). It was integrated into three modes for
165 the MHD site with the near-hydrophobic mode (NH: $1 < Gf < 1.3$), more hygroscopic
166 mode (MH: $1.3 \leq Gf < 1.85$) and sea salt mode (SS: $Gf \geq 1.85$) for further examination
167 (Xu et al., 2021a).

168 –Here for each particle size, the hygroscopicity parameter κ can be subsequently
169 calculated using κ -Köhler theory (Petters and Kreidenweis, 2007):

$$170 \quad \kappa = (Gf^3 - 1) \cdot \left[\frac{1}{RH} \exp\left(\frac{4\sigma_s M_w}{RT\rho_w D_d Gf}\right) - 1 \right] \quad (1)$$

171 where RH is the HTDMA relative humidity (90% set in the instrument), $\sigma_{s/a}$ is the
172 surface tension of pure water (0.072 mN m⁻¹), M_w and ρ_w are the molecular weight and
173 the density of pure water, R is the gas constant, and T is the absolute temperature, D_d is
174 the droplet diameter.

175 Then, the κ -PDF is obtained and normalized as $\int_0^\infty c(\kappa)d\kappa = 1$, where $c(\kappa)$ is
176 normalized as κ -PDF. Further it was used to calculate the particle population
177 heterogeneity (Calculation seen in Section 2.3).

178 **Chemical components**

179 For the inland atmospheric measurements, the non-refractory submicron aerosol
180 (smaller than 1 μ m, NR-PM₁) chemical composition was quantitatively characterized
181 using the Aerodyne High-Resolution Time-of-Flight Aerosol Mass Spectrometer (HR-
182 ToF-AMS) (DeCarlo et al., 2006), including sulfate (SO₄²⁻), nitrate (NO₃⁻), ammonium
183 (NH₄⁺), chloride (~~Ch~~Chl) and organics (Org). The black carbon (BC) mass
184 concentration was determined from the light absorption with a seven-wavelength
185 aethalometer (AE33, Magee Scientific Corp.).

186 –Measurements of PM₁ in the coastal atmosphere were also performed by the HR-
187 ToF-AMS, including major inorganic salts (non-sea-salt sulfate, nss-SO₄²⁻;
188 methanesulfonic acid, MSA; NO₃⁻; NH₄⁺) and organic matter. The instrument operation
189 and calibration have been described in previous studies (Ovadnevaite et al., 2014; Xu

190 et al., 2019).

191 **Aerosol number size distribution and CCN number concentration**

192 Particle number size distributions (PNSD) were measured using an integrated
193 system consisting of a Differential Mobility Analyzer (DMA; model 3081, TSI Inc.)
194 coupled with a Condensation Particle Counter (CPC; model 3772, TSI Inc.). During the
195 measurements at IAP, the PNSD covered the size range of 10-550 nm with a 5-minute
196 time resolution. It scanned size range of 20-500 nm at MHD with a 10-minute temporal
197 resolution. The CCN number concentrations were quantified at both sites using a
198 Droplet Measurement Technologies CCN counter (DMT-CCNc) (Lance et al., 2006).
199 The instrument's supersaturation (SS) settings were carefully calibrated before and after
200 each campaign using ammonium sulfate aerosol following Rose et al. (2008). Four
201 effective supersaturations (SS) were 0.14%, 0.23%, 0.40% and 0.76% at IAP site. Four
202 SS levels were 0.25%, 0.5%, 0.75% and 1% at MHD site with an uncertainty of $\pm 0.03\%$.
203 Using measurements at set supersaturation of 0.2% as an example explores the CCN
204 activity in the following discussions.

205 **2.3 Calculation the heterogeneity for aerosol particles**

206 To characterize the heterogeneous distribution of the hygroscopic and non-
207 hygroscopic components in populations (Chen et al., ~~2022~~2022b), we calculated the
208 mixing state index (χ) using the κ -PDF, following the methodology of Yuan et al. (2023).
209 Two surrogate groups in a population of N aerosol particles were assumed (Zheng et al.,
210 ~~2021~~2021a). One surrogate group consists the non- and/or slightly hygroscopic species

211 with $\kappa_{NH}\kappa_N$ of ≤ 0.0105 and another group contains the more hygroscopic species with
 212 κ_H of 0.5-0.6 (Yuan et al., 2023; Ching et al., 2017). At, referred inorganics). Ambient
 213 particles typically contain one or two of the coastal MHD site, we accounted
 214 for components and the κ lies between 0 and 0.6 at IAP or 0.8 at MHD as shown in
 215 Figure S1. Taking into account the enhanced hydrophilicity of marine aerosols by
 216 additionally testing at MHD site, calculation assuming κ_H values of 0.7 and 0.8 (were
 217 shown in Fig. S1)-S2. While these variations in κ_H introduced a mean uncertainty of
 218 8% in χ values, it did not significantly affect the seasonal or site comparisons. The
 219 volume fraction of two surrogate groups can be calculated based on the total κ
 220 according to the Zdanovskii–Stokes–Robinson (ZSR) mixing rule (Zdanovskii, 1948;
 221 Stokes et al., 1966).

222 The mixing state index χ is defined as the affine ratio of the average particle species
 223 diversity ($D\alpha$) and population species diversity ($D\gamma$) as:

$$224 \quad \chi = \frac{D\alpha - 1}{D\gamma - 1} \quad (2)$$

225 The average per-particle species diversity $D\alpha$ can be calculated as follows. First,
 226 the mixing entropies at bin i (H_i) are determined according to equation (3),

$$227 \quad H_i = -P_{i,NH}P_{i,N} \times \ln P_{i,NH}P_{i,N} - P_{i,H} \times \ln P_{i,H} \quad (3)$$

228 where $P_{i,NH}$ and $P_{i,H}$ are the volume fraction of each group for the κ -PDF with X bins
 229 at bin i ($i=1,2,\dots,X$), and can be determined from the $P_{i,NH}P_{i,N} + P_{i,H} = 1$ and
 230 $P_{i,NH}P_{i,N} \times \kappa_{NH}\kappa_N + P_{i,H} \times \kappa_H = \kappa_i$. Here $\kappa_{NH}\kappa_N = 0.01$, $\kappa_H = 0.6$; κ_i represents
 231 the hygroscopicity parameter at bin i .

232 Based on the assumption that particles in the same diameter have the same mixing

233 entropy $H_\alpha = \sum_{j=1}^N P_j \times H_j$, $P_j = \frac{V_j}{V_{total}} = \frac{1}{N}$; the per-particle mixing entropies H_α is
 234 determined according to equation (4),

$$235 \quad H_\alpha = \sum_{i=1}^X H_i \times c(\kappa)_i \times \Delta\kappa \quad (4)$$

236 where $c(\kappa)_i$ is the probability density of the normalized κ -PDF at bin i , and $\Delta\kappa$
 237 represents the bin width. Then, the average per-particle species diversity D_α can be
 238 determined as $D_\alpha = e^{H_\alpha}$;

239 The bulk population species diversity D_γ can be calculated as follows. First, the
 240 aerosol population of the mixing entropy can be calculated as equation (5):

$$241 \quad H_\gamma = -P_{NH}P_N \times \ln P_{NH}P_N - P_H \times \ln P_H \quad (5)$$

242 where $P_{NH}P_N$ and P_H are the volume fraction of the non-hygroscopic and hygroscopic
 243 components in the population, and can be calculated by equation (6) and (7):

$$244 \quad P_{NH}P_N = \sum_{i=1}^X P_{i,NH}P_N = \sum_{i=1}^X P_{i,N} \times c(\kappa)_i \times \Delta\kappa \quad (6)$$

$$245 \quad P_H = \sum_{i=1}^X P_{i,H} \times c(\kappa)_i \times \Delta\kappa \quad (7)$$

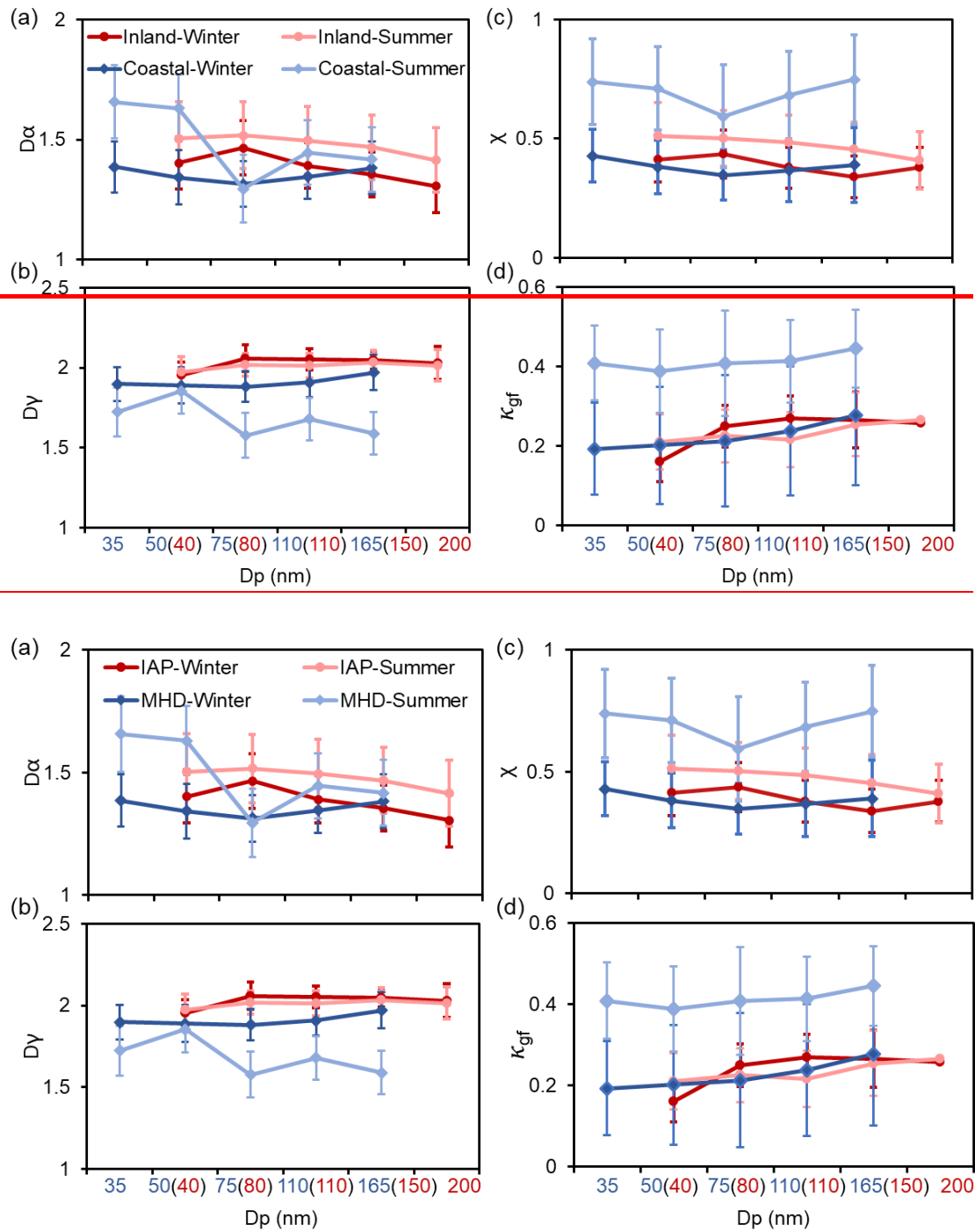
246 Then, the bulk population species diversity D_γ can be determined as $D_\gamma = e^{H_\gamma}$.
 247 Here, the definition of surrogate species as supersets encompassing hygroscopicity
 248 heterogeneity implies that the heterogeneity parameter χ ranges from 0 to 1. When the
 249 mixing index χ approaches 0, it indicates a completely segregated state where
 250 hygroscopic and non-hygroscopic species reside in distinct particles. While for the case
 251 the mixing index χ to be 1 represents that the non-hygroscopic and hygroscopic species
 252 distributing homogeneously throughout the aerosol population.

3. Result and Discussion

3.1 Comparison of the heterogeneity in the inland and coastal atmosphere

To characterize the hygroscopic heterogeneity of atmospheric aerosols, Figure 2 depicts variations in mixing state metrics (D_α , D_γ , χ) and the hygroscopic parameter (κ_{gf}) across particle size distributions. ~~For inland aerosols, The~~ D_α and χ decrease with increasing particle diameter, accompanied by higher κ_{gf} values at IAP site. This trend indicates that inland particle populations tend to homogenize into hygroscopic compositions through primary particle aging or secondary formation processes (Liu et al., 2025; Chen et al., ~~2022~~2022b; Zhong et al., 2022). In contrast, ~~coastal~~ particles exhibit a non-monotonic pattern at MHD site: D_α and χ decrease for Aitken-mode particles (<100 nm) but increase for accumulation-mode particles. The κ_{gf} shows consistent size-dependent increases in both winter and summer campaigns.

Notably, the mixing state metrics exhibit a pronounced minimum at 75 nm particles, influenced by distinct mechanisms: winter minima reflect the high sea salt fraction, while summer minima are driven by anthropogenic organic matter (Cheung et al., 2020; Xu et al., 2021a). Lower winter χ values—coupled with broader κ -PDF distributions—indicate stronger external mixing and compositional diversity compared to summer (Fig. S2S1). Seasonal χ and κ_{gf} disparities are more pronounced at ~~the~~ coastalMHD site, primarily driven by the seasonal alternation of marine and anthropogenic emission sources.



273

274

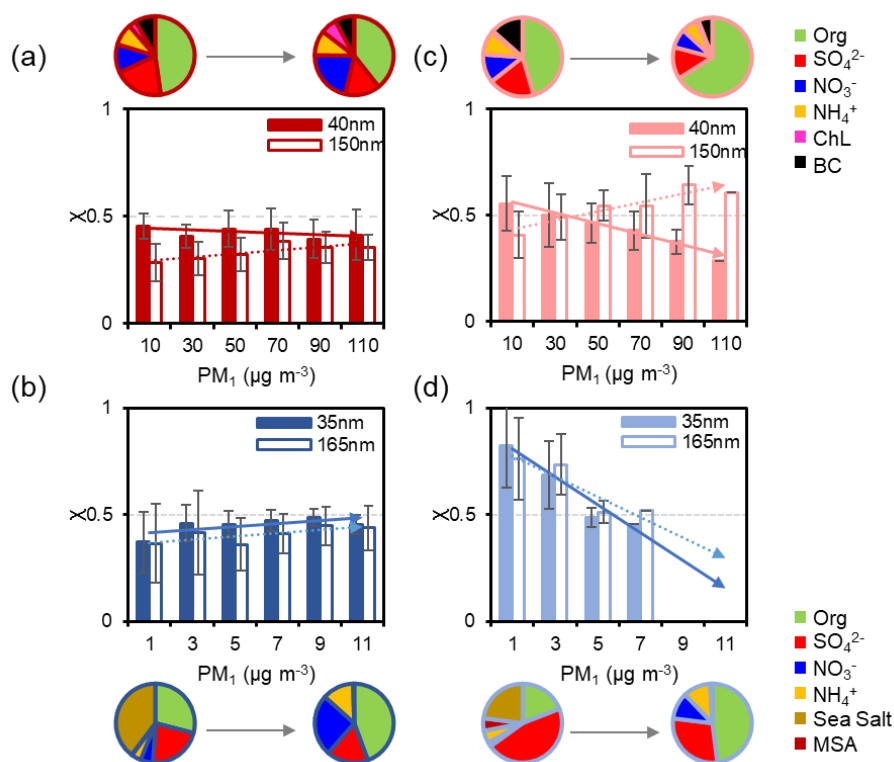
275 **Fig 2.** Mean values of the $D\alpha$ (a), $D\gamma$ (b), χ (c) and κ_{gf} (d) for aerosols of five diameters

276 during winter and summer periods **in Inland (at IAP)** and **Coastal (Mace Head)** sites.

277 Ultrafine particles (40 nm **inland in IAP** vs. 35 nm **coastal in MHD**, Aitken mode)

278 and larger particles (150 nm **inland in IAP** vs. 165 nm **coastal in MHD**, accumulation

279 mode) ~~were~~are selected to investigate distinct evolutionary processes of aerosol
280 heterogeneity (Fig. 3 and Fig. S3). With the increasing of ~~PM~~PM₁ concentration during
281 winter, the variation in χ values exhibit only minor both at the ~~inland~~IAP and
282 ~~coastal~~MHD sites, generally fluctuating between approximately -0.04 and 0.08 (Fig.
283 3a and b). Inland accumulation-mode particles show a modest increase in χ ,
284 corresponding with a higher proportion of inorganic salts. Conversely, at ~~coastal~~
285 ~~sites~~MHD site, the composition fraction shifts from a sea-salt dominance toward
286 organic matter, accompanied by a $\sim 20\%$ increase in nitrate content (Fig. 3b). In summer,
287 the variation of χ with PM concentration becomes markedly pronounced at both
288 ~~inland~~IAP and ~~coastal~~MHD stations. For example, χ for 40 nm particles decreases as
289 PM increases at ~~inland~~sitesIAP site (Fig. 3c). The elevated particle heterogeneity
290 mainly arises from the locally primary emissions ~~and photochemically driven new~~
291 ~~particle formation, corresponding to the enhanced primary organic emissions as shown~~
292 ~~in Fig. S4. It appeared more pronounced during evening rush hours~~. In contrast, χ for
293 150 nm particles increases from ~ 0.40 to ~ 0.60 with rising PM, reflecting enhanced
294 secondary formation and internal mixing during pollution process that render the
295 particle population more homogeneous. At coastal sites, χ declines with rising PM by
296 approximately 0.37 for 35 nm particles and 0.24 for 165 nm particles, mirroring the
297 shift in chemical composition makeup from inorganic dominance to greater organic
298 content (Fig. 3d).

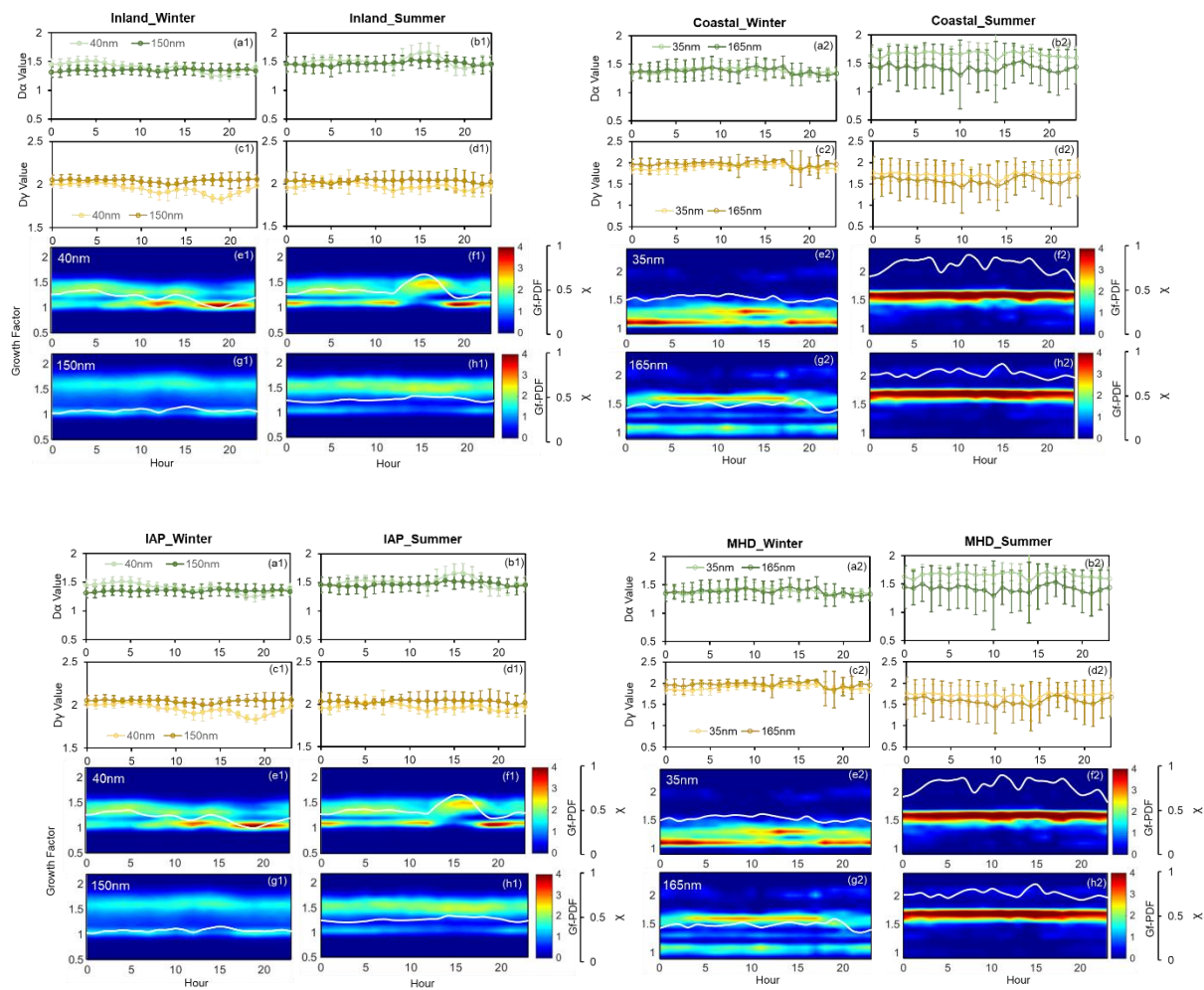


299

300 **Fig 3.** Variation of the average χ for 40 nm and 150 nm in inland particles at IAP and
 301 35 nm and 165 nm in coastal at MHD site with the particle mass concentration in
 302 Inland IAP-winter (a), Inland IAP-summer (b), Coastal MHD-winter (c) and
 303 Coastal MHD-summer (d). The pie charts represent the average mass fraction during
 304 four field campaigns measurements.

305 Figure 4 illustrates pronounced diurnal variations in of mixing state metrics
 306 ($D\alpha$, $D\gamma$, Gf-PDF, χ) between inland and coastal atmospheres. χ at IAP and MHD sites
 307 are shown in Figure 4. In the inland atmosphere, IAP-winter, particles exhibited steeper
 308 declines in $D\alpha$ and χ during evening rush hours than summer, indicating a higher
 309 fraction of non-hygroscopic particles (40 nm) from fresh traffic emissions (Fig. 4a1 and
 310 S4). Concurrently, reduced $D\gamma$ values suggest that the bulk population consists of
 311 uniformly distributed less-hygroscopic (LH) components (Fig. 4c1). Aitken mode

312 particles showed bimodal and broader Gf-PDF distributions, corresponding to cooking
313 activities (11:00–13:00 LT) and traffic peaks (17:00–20:00 LT) (Cai et al., 2020).
314 Midday photochemical aging promoted more internally mixed aerosols (Yang et al.,
315 2012; Liu et al., 2025), as evidenced by increasing D_{α} at the urban site (Fig. 4b1).
316 Conversely, the γ for accumulation-mode particles showed minimal diurnal variations;
317 suggesting stable relative proportions of LH both in IAP-winter and more-IAP-summer.
318 This is mainly due to the dominant hygroscopic (MH) components in inland aerosols
319 aeross seasons mode for 150 nm particles (Fig. 4g), especially during summer, which
320 is mainly from secondary formation or aging of the primary particles (such as the
321 transformation from primary organic aerosol (POA) to secondary organic aerosol (SOA)
322 in Fig. S4) (Wang et al., 2019; Fan et al., 2020).



323

324 **Fig 4.** The Diurnal variation of $D\alpha$, $D\gamma$, Gf-PDF, and χ during winter and summer
 325 periods for 40 nm and 150 nm aerosols in Inland at IAP (a1-h1) and for 35 nm and 165
 326 nm aerosols Coastal/MHD site (a2-h2).

327 For the coastal atmosphere, the mixing state metrics ($D\alpha$, $D\gamma$, and χ) of Aitken and
 328 accumulation mode particles in winter exhibited analogous diurnal patterns,
 329 characterized by a descending trend at nightfall- (Fig. 4a2-h2). This corresponds to an
 330 enhanced modal distribution of near-hydrophobic (NH) particles at 35 nm and more-
 331 hygroscopic (MH) particles at 165 nm. In summer, $D\alpha$ and $D\gamma$ both trended downward
 332 during daytime, with the decline of $D\gamma$ being more pronounced. A conspicuous seasonal

333 discrepancy between Aitken and accumulation mode particles was observed in this
334 region (Fig. 4a2–h2), where the mixing state index χ increased incrementally from
335 winter to summer. Specifically, the mean χ for 35 nm particles escalated from 0.42 to
336 0.80, and for 165 nm particles, it rose from 0.39 to 0.76. This trend demonstrates a
337 strong alignment with the spread factor (used as a measure of particle mixing state)
338 documented by Xu et al. (2021a,~~b~~).

339 ~~The~~ Similar to the mixing state χ , a very clear seasonal pattern of the aerosol
340 hygroscopic distribution was found (Fig. 4e-h). In winter, the Gf-PDF diurnal profiles
341 of both Aitken and accumulation mode particles ~~displayed~~ showed bimodal ~~and~~
342 ~~broadened~~ distribution, ~~corresponding to a less-~~ (Fig. 4e2-g2) as evident by the number
343 fraction of nearly-hydrophobic and more hygroscopic ~~(LH)~~ modes (Fig. S5). The NH
344 mode ~~of~~ was likely to be the anthropogenic organic matter and biogenic origin ~~during~~
345 ~~nighttime and a more-hygroscopic (MH) from marine mass (Xu et al., 2020), especially~~
346 for the Aitken mode ~~dominated by~~. The more hygroscopic and sea salt ~~(comprising 55%~~
347 ~~number fraction) during daytime. mode was mostly contributed from the nss-sulfate and~~
348 sea salt in winter (Xu et al., 2021a). Analogously, accumulation mode particles
349 ~~exhibited bimodal distributions~~ with a higher proportion of MH and SS mode ~~during~~
350 ~~daytime,~~ (Fig. S5) primarily attributed to the prevalence of ~~sea salt and~~ non-sea-salt
351 sulfate (nss-sulfate) and sea salt in the coastal atmosphere (Xu et al., ~~2020~~). 2020. The
352 bimodal and broad of hygroscopic distribution suggested that particles were more
353 diverse and external mixed, consistent with the lower χ value in winter.

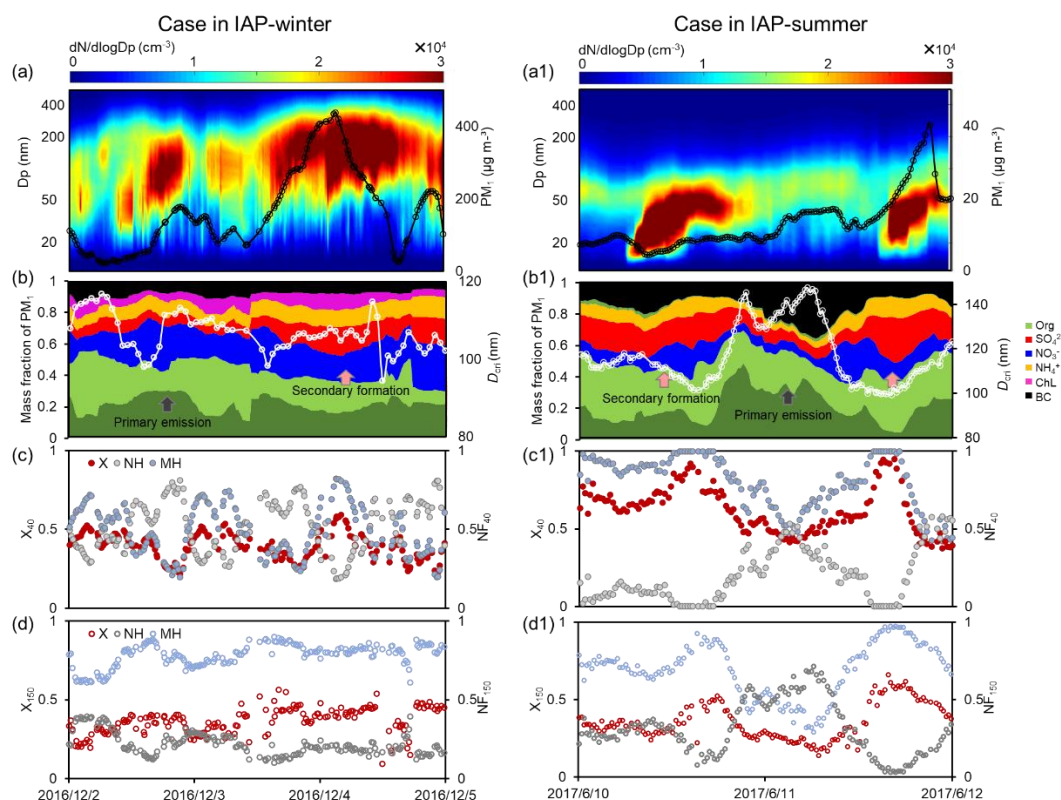
354 In contrast, summer observations revealed that Gf-PDFs of both Aitken and

355 accumulation mode particles transitioned to unimodal distributions, signifying particles
356 in summer had more homogeneous composition with a large extent of internal mixing
357 of LH particles (with higher γ). Such diurnal trend in Gf-PDFs was consistent along
358 with the high number fraction of MH-mode and MH components within individual
359 particles. This uniformity is linked to processes including sulfuric acid condensation,
360 admixture low NH-mode (Fig. S5). The higher hygroscopicity and MH mode in summer
361 were largely driven by the enhancement of sulfate with biogenic and decrease of organic
362 matter (Xu et al., 2021a), as well as Fig. S5. And a clear shift from NH to MH mode at
363 midday might further demonstrate the promotion of photochemical oxidation and
364 atmospheric aging (Jimenez in summer (Xu et al., 2009), 2021a).

365 **3.2 Dependence Impacts of Primary Aerosol Emissions and Secondary Aerosol** 366 **Formation on Aerosol Mixing State**

367 As already noted above, changes in γ were clearly associated with the aerosol
368 properties on chemical composition varying with site and season. The relationships
369 between the mixing state index and the number fraction of hydrophobic and
370 hygroscopic mode during four campaigns are presented in Figure S6. The γ exhibited
371 negative correlations with the fraction of hydrophobic mode but a positive relationship
372 with the fraction of hygroscopic particles, highlighting the markedly different effects
373 of the primary emissions and secondary formation on aerosol mixing state (Tao et al.,
374 2024). To gain more insight on this effect between inland and coastal atmosphere, four
375 case are analyzed (Fig. 5 and 6): case for IAP-winter, case for IAP-summer, case for
376 MHD-winter and case for MHD-summer.

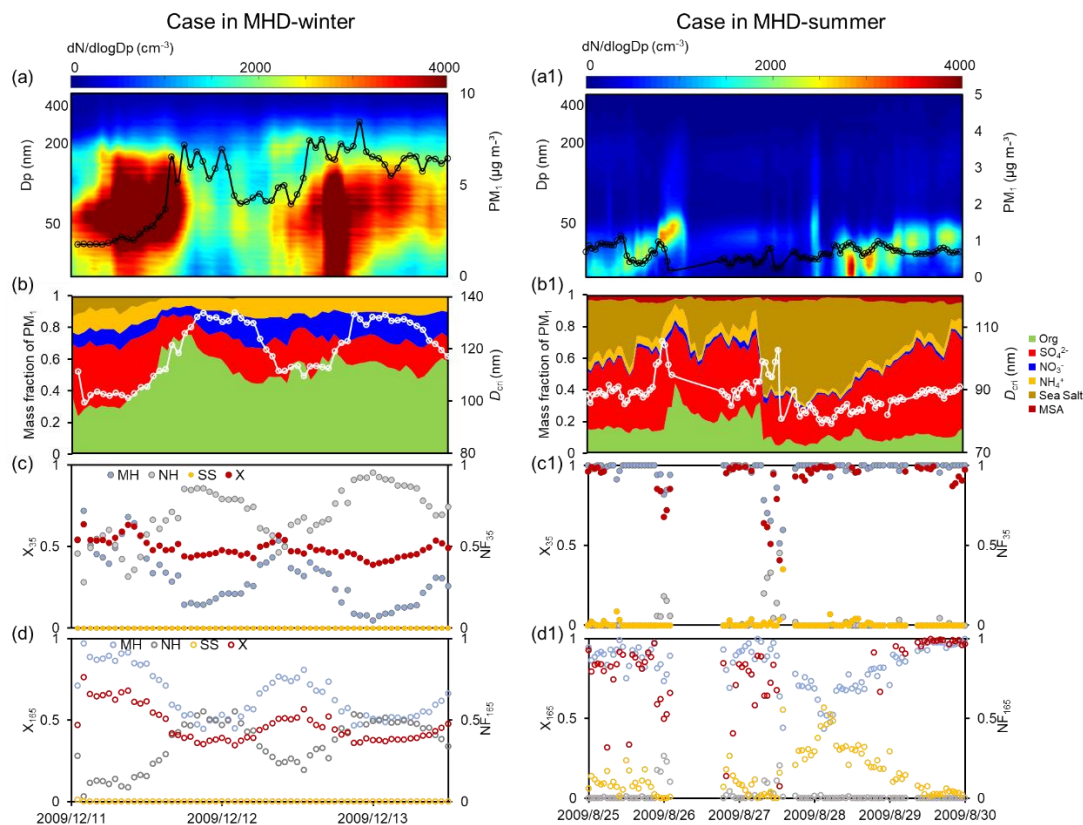
377 Case for IAP-winter is a heavy polluted event with the mean PM mass
 378 concentration increased from 22 to 437 $\mu\text{g m}^{-3}$ (Fig. 5a-d). The 40- and 150-nm χ
 379 patterns shifted quickly during the pollution periods. With the mass fraction of
 380 hydrophobic compounds (ie., POA) in PM_{10} increased, the χ of 40-nm particles
 381 decreased from 0.5 to 0.2, that is, an enhanced NH mode and a weakened MH mode (Fig.
 382 5b-c). At this stage, large particles for 150 nm are mainly from aqueous formation with
 383 more proportion of nitrate. The corresponding χ of 150 nm was higher. While with that
 384 the mass fractions of secondary organic and inorganic compositions increased, particles
 385 were more internal mixed with χ increased to be 0.6 for 40-nm and 0.53 for 150-nm
 386 particles.



387
 388 **Fig 5.** Case in IAP-winter and IAP-summer. Particle number size distribution and PM_{10}
 389 (a), mass fraction of the PM_{10} and the critical diameter (D_{crit}) (b), mixing state index (χ),

390 number fraction of the nearly hydrophobic mode (NH) and more hygroscopic mode
391 (MH) for 40 nm particles (c), χ , NH and MH for 150 nm particles (d).

392 Case for IAP-summer is the typical new particle formation events (NPF) with the
393 mean PM_{10} of $13 \mu\text{g m}^{-3}$ (Fig. 5a1-d1). With the evolution of NPF events, the χ of 40-
394 and 150-nm particles increased to be 0.95 and 0.61 with the enhanced proportion of
395 more-hygroscopic components (ie., SOA, NO_3^- , SO_4^{2-}). The χ pattern is opposite of that
396 the number fraction of NH mode and consistent with the variation of MH mode (Fig.
397 S6). Note that a sudden decrease in χ on June 11th was disturbed by the strong primary
398 emission. The chemical mass fractions showed more POA and black carbon with an
399 enhanced NH mode and a weaker MH mode (Fig. 5b1-d1). The χ of 40-nm particles
400 decreased to be 0.4 and that of the 150-nm particles decreased to be 0.2. The χ patterns
401 appear to similar transitions for Aitken and accumulation-mode particles during haze
402 and NPF events. The increase in χ is synchronous with the increase in MH mode from
403 secondary formation but opposite with that of LH mode from primary emissions. This
404 implies that the primary emissions would lead particles more external mixing while
405 secondary formation would promote aerosol more internal mixed in Inland atmosphere.



406

407 **Fig 6.** Case in MHD-winter and MHD-summer. Particle number size distribution and
 408 PM_{10} (a), mass fraction of the PM_{10} and the critical diameter (D_{crit})(b), mixing state index
 409 (χ), number fraction of the nearly hydrophobic mode (NH) and more hygroscopic mode
 410 (MH) for 35 nm particles (c), χ , NH and MH for 165 nm particles (d).

411 Case for MHD-winter is a high organic matter pollution event with the mean PM_{10}
 412 of $5.2 \mu\text{g m}^{-3}$ and 52% mass fraction of organics (Fig. 6a-d). Larger presence of
 413 anthropogenic organic matter resulted the NH mode for 35-nm particles to be 95% and
 414 165-nm particles to be 53% (Fig. 6). The χ of 35- and 165-nm particles decreased with
 415 the NH mode increased (Fig. S6), similar with the case for IAP site. There was a steady
 416 increase in χ when the MH-mode particles started increasing with the increase in mass
 417 fraction inorganics, eg., 35 nm particles showed the mean χ increasing from 0.43 to

418 0.57 and 165 nm particles from 0.35 to 0.6. This indicated that the trend of aerosol
419 mixing state closely followed the evolution emission and secondary formation.

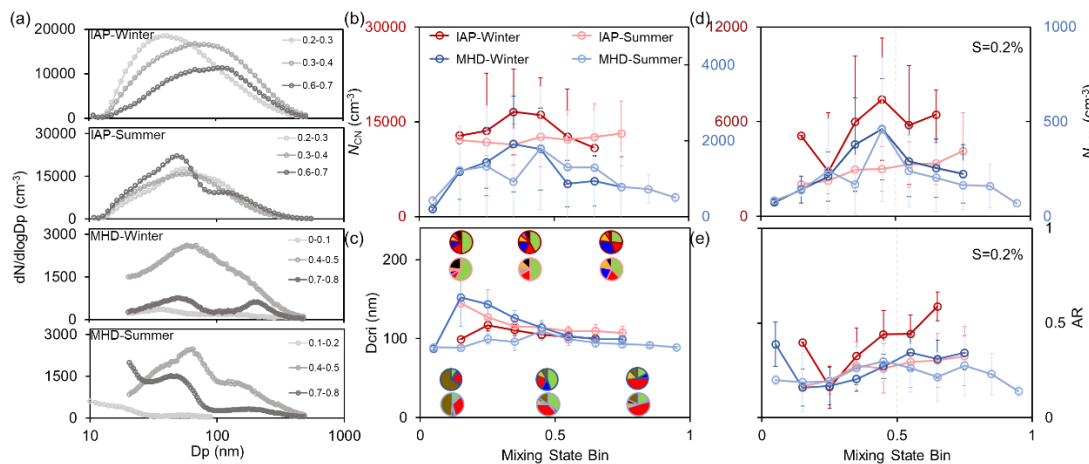
420 Case for MHD-summer is an extremely clean event with the mean PM₁ of 0.7 μg
421 m⁻³ (Fig. 6a1-d1). The dominated MH mode was found throughout the case, which
422 could be attributed from the high mass fraction of nss-sulfate (41% average). Compared
423 with the case in MHD-winter, the mean proportion of organic has decreased to be 15%.
424 Therefore, the χ remains at a high value (mean χ of 0.9 for 35-nm and 0.8 for 165-nm
425 particles). Until August 28th, a stronger increase in the mass fraction of sea salt and
426 accordingly SS mode in larger-size particles was observed. The χ decreased rapidly
427 with the decrease in MH mode and enhanced SS mode, especially for the accumulation
428 mode particles, suggesting the sea spray production makes particles more externally
429 mixed.

430 In summary, these results suggest that the primary emission and secondary
431 formation drive the hygroscopic distribution and can result in significant variation of
432 aerosol mixing state χ both in Inland and coastal atmosphere. The pattern of χ varied
433 among site and season, highlighting the importance of considering the impact of mixing
434 state on CCN activity.

435 **3.3 Impact of Mixing State on CCN Activity**

436 The mixing state of particle populations undergoes dynamic transformations
437 during atmospheric aging, profoundly influencing their CCN activity. Unlike prior
438 studies that assumed mixing states based on chemical component fractions (Yang et al.,

439 2012; Padró et al., 2012; Ren et al., 2018), this work employs the entropy-derived
 440 mixing state index χ , which quantifies the distribution of hygroscopic and non-
 441 hygroscopic species (Zheng et al., 2021a; Ching et al., 2017). ~~We systematically~~
 442 ~~investigate how aerosol properties evolve~~The variations of particle size and chemical
 443 ~~composition~~ with ~~changing χ~~ . Figure 5 illustrates the dependency of aerosol
 444 ~~characteristics on increments of χ~~ (ranging from 0 to 1 in 0.1 increments), with the step
 445 ~~of 0.1~~ are illustrated in Figure 7, presenting key insights into particle size and chemical
 446 ~~composition~~ of two fundamental determinants of CCN activity (RenDusek et al.,
 447 ~~2018~~).

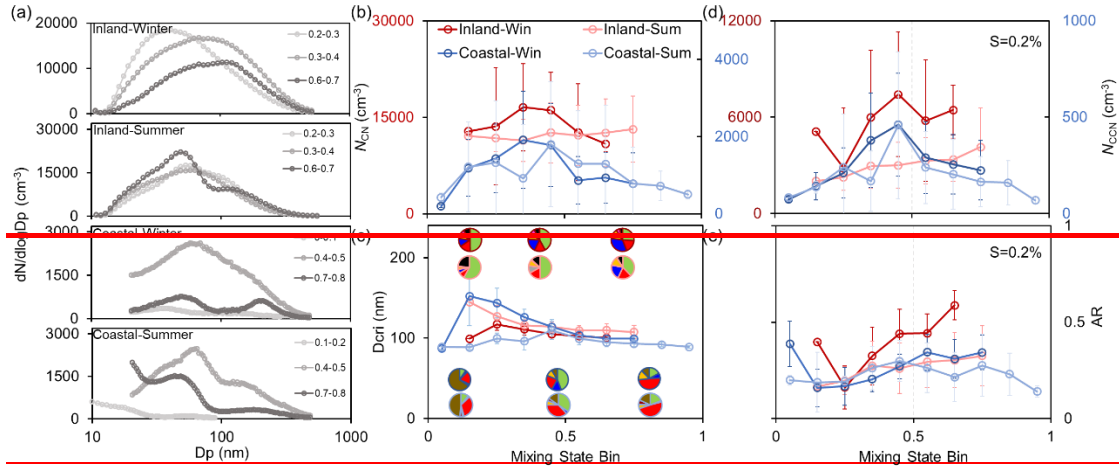


448 **Fig 7.** Comparison of the average particle number size distribution (PNSD) in different
 449 mixing state index (χ) (a), CN number concentration (N_{CN}) as a function of χ (b),
 450 Critical diameter (D_{crit}) at $S=0.2\%$ and mass fraction of chemical composition as a
 451 function of χ (c), CCN number concentration (N_{CCN}) (d) and activation ratio (AR) at
 452 $S=0.2\%$ a function of χ (e).

454 As χ increases, the peak diameter (D_{peak}) of the particle number size distribution
 455 (PNSD) shifts toward larger sizes (Fig. 5a7a and Fig. S4S7), while peak concentrations

456 occur within the intermediate χ range (0.3–0.6). This trend indicates that CN number
457 concentration (N_{CN}) first increases, driven by primary emissions and new particle
458 formation, then decreases due to mixing and aging processes (Fig. ~~5b7b~~). Notably,
459 ~~inland new particle formation events frequently occurred in IAP-summer (Fig. S8),~~
460 ~~corresponding the gradually increase of χ . And the χ for Aitken-mode is significantly~~
461 ~~larger than the accumulation-mode particles during this period. Thus, N_{CN} exhibits a~~
462 ~~sustained slight increase, linked to frequent new particle formation events and~~
463 ~~subsequent particle growth. as the degree of the internal mixing increases in IAP-~~
464 ~~summer.~~

465 The critical diameter (D_{cri})—defined as the minimum size for activation at a given
466 supersaturation—depends on ~~aerosol hygroscopicity. This hygroscopicity is determined~~
467 ~~by both the hygroscopicity and~~ the mass fraction of soluble components (Petters and
468 Kreidenweis, 2007). Using ~~a typical cloud measurements at~~ supersaturation of 0.2% as
469 ~~a case study an example~~, Fig. ~~5e7c~~ shows that D_{cri} decreases with increasing ~~soluble~~
470 ~~species highly hygroscopic inorganic components~~ (e.g., sulfate, nitrate) in the inland
471 atmosphere. In contrast, coastal D_{cri} exhibits nonlinear variations with χ : high external
472 mixing (low χ) elevates D_{cri} due to dominant organic components, reducing sea salt
473 particle fractions. As χ increases, the mass fraction of non-sea-salt sulfate (nss-sulfate)
474 rises, enhancing activation potential by decreasing D_{cri} .



475

476 **Fig 5.** Variation of the average particle number size distribution (PNSD) with the
 477 mixing state index χ (a), variation of the N_{CCN} with the χ (b), variation of the D_{crit} and
 478 mass fraction of chemical composition with the χ (c), variation of the N_{CCN} and
 479 activation ratio (AR) at $S=0.2\%$ with the χ (d-e).

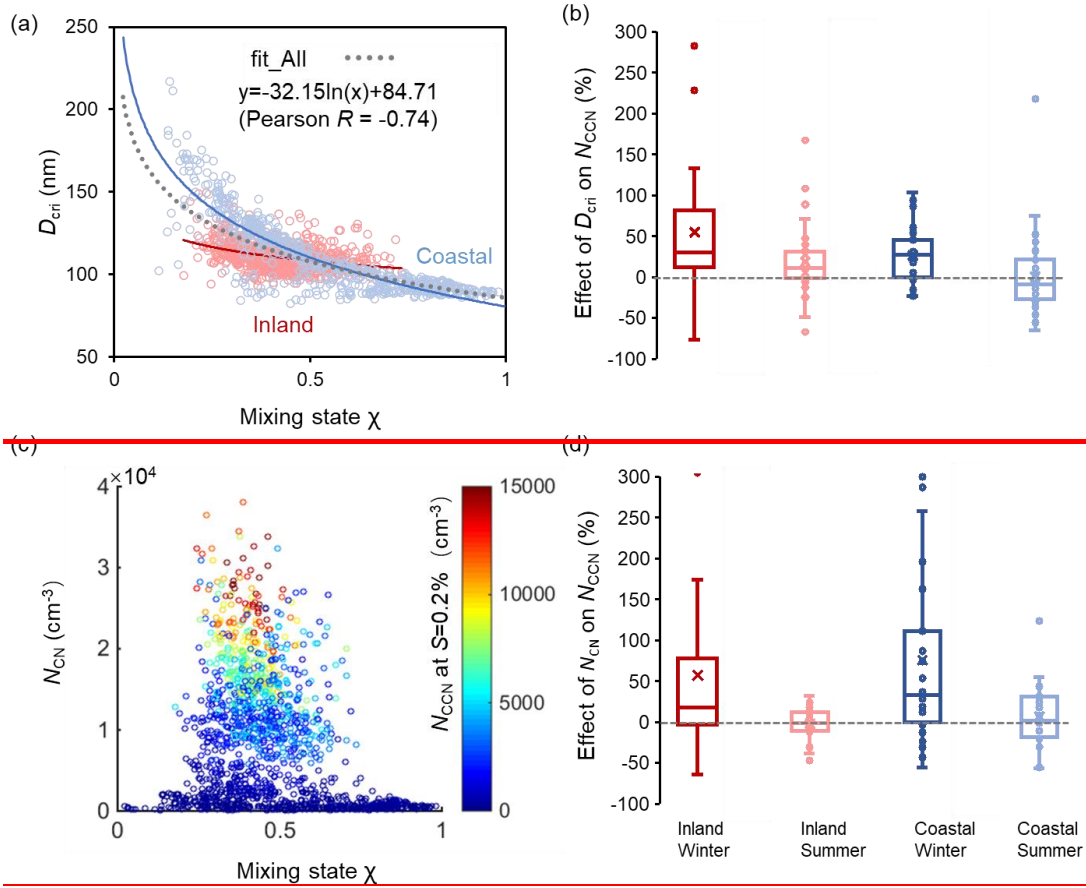
480 The dependence of CCN activity at 0.2% supersaturation on mixing state index χ
 481 reveals distinct inter-atmospheric differences, as shown in Fig. 5d7d-e. In the inland
 482 atmosphere, N_{CCN} at $S=0.2\%$ demonstrates a monotonic increasing trend with χ ,
 483 attributed to the synergistic effects of rising N_{CN} and decreasing D_{crit} (Fig. 55S9). By
 484 contrast, coastal N_{CCN} follows a pattern analogous to N_{CN} , with peak concentrations
 485 shifting toward higher χ values. This highlights the dominant role of particle size effects
 486 in enhancing CCN concentrations under marine-influenced conditions (PerkinsDusek
 487 et al., 20222006).

488 Two distinct D_{crit} - χ trends underpin these disparities: one remains stable, driven by
 489 the inherent hygroscopicity of sea salt, while the other exhibits steep D_{crit} declines
 490 associated with anthropogenic pollution as internal mixing intensifies. These
 491 discrepancies are further manifested in the nonlinear D_{crit} - χ relationship. The activation

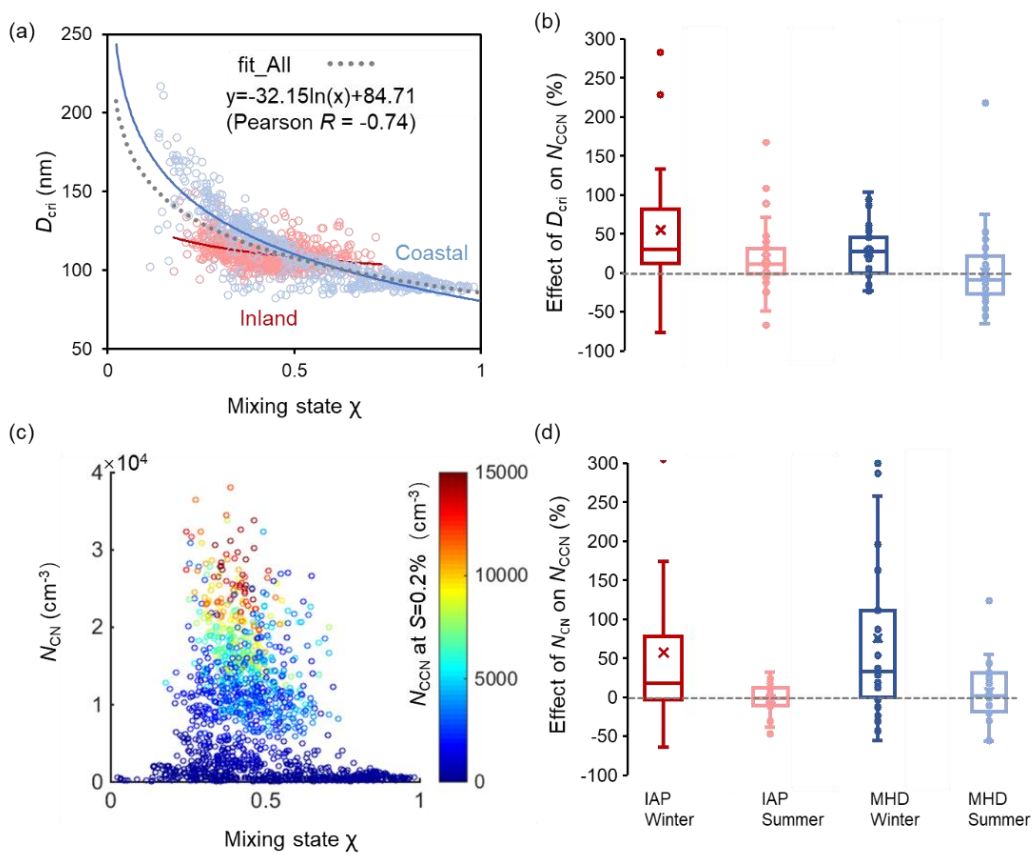
492 ratio (AR)—quantifying aerosol cloud droplet formation potential at fixed
493 supersaturation—also varies by site (Fig. [5e7e](#)). Notably, ~~inland-winter~~ AR shows a
494 marked increase with χ [in IAP-winter](#), likely due to enhanced N_{CCN} from the elevated
495 inorganic fraction under higher mixing states (Fig. 3). Conversely, the inorganic
496 fraction decreases during other sampling periods, dampening AR growth.

497 ~~3.3 Impact of the mixing state on the CCN activity~~

498 To better interpret the impact of mixing state on CCN concentrations, Fig. [68](#)
499 quantifies the relative change in N_{CCN} at $S=0.2\%$ as mixing state index χ increases,
500 contextualizing how CN concentration and chemical compositions (i.e., D_{cri}) evolve
501 with mixing and aging across particle populations. D_{cri} demonstrates heightened
502 sensitivity to minor χ fluctuations at low mixing states ($\chi < 0.5$; Fig. [6a8a](#)), whereas
503 further increases in internal mixing (higher χ) exert negligible influence on D_{cri} for
504 already internally mixed particles. This behavior suggests that the D_{cri} - χ relationship
505 may enable a novel parameterization for D_{cri} estimation, a framework that is not yet
506 reported in prior literature.



507



508

509 **Fig 68.** Dependency of the critical diameter (D_{crit}) on the χ (a), relative change of CCN

510 number concentration (N_{CCN}) at supersaturation $S = 0.2\%$ with the reduction in D_{crit} (b);
511 Dependency of the CN number concentration (N_{CN}) on the χ , different colors represent
512 the N_{CCN} (c), relative change of N_{CCN} with the change in N_{CN} (d).

513 ~~Coastal aerosol~~Aerosol data points at MHD site (blue dots) span a broad D_{crit} range
514 (80–220 nm) with χ varying from 0.1 to 1, reflecting alternating influences of highly
515 hygroscopic inorganic salts (sea salt, sulfate) and less-hygroscopic organic matter. In
516 contrast, ~~inland~~ aerosols—dominated by anthropogenic pollutants—exhibit a narrower
517 D_{crit} range (90–150 nm). at IAP site. Both environments show negative D_{crit} - χ
518 correlations, but with distinct functional forms: ~~coastal~~MHD aerosols feature an
519 exceptional logarithmic fit ($D_{crit} = -42.98\ln(\chi) + 80.36$, $R^2 = 0.75$; Fig. ~~6a~~8a blue line),
520 while ~~inland~~IAP aerosols (red line) yield a shallower slope (-12.04). Pooling all data,
521 we derive a generalized parameterization: $D_{crit} = -32.15\ln(\chi) + 84.71$ (Pearson $r = -0.74$,
522 $R^2 = 0.54$). As already discussed above, strong impact of primary emission and
523 secondary formation on aerosol mixing state was observed in both sites (Fig. 5 and 6).
524 It also provides even more details on the D_{crit} - χ correlations. For example, the D_{crit}
525 exhibited rapidly increased with the primary emissions (ie., mass fraction of POA
526 enhanced) during polluted periods. The D_{crit} pattern appeared opposite with that of the
527 mixing state index, especially for the accumulation-mode particles. More pronounced
528 D_{crit} - χ correlations were observed during the new particle formation (Fig. 5a1-d1). The
529 decreasing presence of D_{crit} matched the increasing proportion of SO_4^{2-} and SOA with
530 the χ increased during NPF events. Similar correlations between the critical diameter
531 and mixing state index were also found in the coastal atmosphere, especially for the

532 case of the enhanced anthropogenic organic matter and sea salt production (Fig.6). This
533 implies that the relationship between the D_{cri} and χ might be disturbed by the variation
534 of emission pollution and secondary formation processes, resulting in spatiotemporal
535 differences.

536 Box plot analyses (Fig. S6S10) show that the mixing state reduces D_{cri} by 2.2–6.8%
537 across campaigns, with the steepest winter decline. ~~χ impacts on~~ Changes in N_{CN} with
538 differ starkly between environments: positive effects in polluted inland air (+9%) versus
539 negative effects in coastal regions (-2%). ~~Inland aerosols~~ Aerosols in IAP, frequently
540 perturbed by primary emissions and new particle formation, exhibit elevated N_{CN}
541 (peaking at $\chi = 0.2\text{--}0.7$), while ~~coastal~~ MHD N_{CN} remains $\sim 5000 \text{ cm}^{-3}$ across all χ .

542 To isolate the impacts of critical diameter (D_{cri}) and condensation nuclei number
543 concentration (N_{CN}) on CCN activity concentration, we categorized data into two groups:
544 C1 (particles within specific N_{CN} ranges) evaluates N_{CCN} variations driven by $D_{\text{cri}}\text{-}\chi$
545 relationships, while C2 (particles within fixed D_{cri} intervals) assesses $N_{\text{CN}}\text{-}\chi$ effects (Fig.
546 ~~6b8b~~). Relative changes (RC) in D_{cri} , N_{CN} , and N_{CCN} with χ were calculated by
547 comparing successive χ increments (χ_{i+1} vs. χ_i , $i=0,0.1\dots 1$) within defined $N_{\text{CN}}/D_{\text{cri}}$
548 windows.

549 Notably, ~~χ change in~~ N_{CCN} exerts more pronounced effects on ~~N_{CCN} for~~ externally
550 mixed aerosols. For example, ~~coastal-MHD-~~ winter aerosols (high external mixing;
551 $\chi_{\text{mean}}=0.38\pm 0.12$) showed N_{CCN} RCs of 23% (C1) and 72% (C2), whereas ~~coastal-MHD-~~
552 summer aerosols (high internal mixing; $\chi_{\text{mean}}=0.69\pm 0.19$) exhibited negligible effects (-
553 2.5% in C1, 0.9% in C2). Inland atmospheres, despite smaller seasonal χ variations,

554 showed analogous trends: winter N_{CCN} RCs (55% in C1, 57% in C2 for external mixing)
555 exceeded summer values for more internally mixed populations (Fig. [6d8d](#)). These
556 results confirm that hygroscopic heterogeneity strongly influences N_{CCN} under external
557 mixing, aligning with prior work (Ching et al., 2017).

558 ~~Mixing state impacts on~~ With the variation in mixing state index χ , changes in N_{CCN}
559 are most pronounced during winter in both environments, attributed to heightened
560 winter D_{crit} sensitivity to χ : a 0.1 χ increase reduces D_{crit} by 5.2% (winter), boosting N_{CCN}
561 by 39%, versus 2.4% D_{crit} reduction (summer) yielding only 6% N_{CCN} enhancement.
562 Concomitantly, winter $N_{CN-\chi}$ effects on N_{CCN} reach 65%, far exceeding summer
563 responses.

564 Contrasting with prior evaluation methods that oversimplify mixing states (Ren et
565 al., 2018; Xu et al., 2021b), the entropy-based framework adopted herein enables
566 explicit quantification of CCN activity evolution in response to mixing state transitions.

567 ~~Inland Aerosols in IAP-winter aerosols~~ are presumably shaped by intense urban
568 pollution sources—including traffic emissions, residential heating, and cooking
569 activities—thereby enriching the externally mixed particle fraction (Fan et al., 2020;
570 Xie et al., 2020). Analogously, ~~coastal winter~~ aerosols in MHD-winter exhibit dominant
571 external mixing, consisting of near-hydrophobic and hydrophilic particle mixtures (Xu
572 et al., 2021a). As illustrated in Fig. [S2S1](#), winter aerosol populations display bimodal
573 or multimodal κ -PDF distributions, evidencing high-degree external mixing with
574 chemically diverse compositions. These results collectively highlight the pivotal role
575 of mixing state heterogeneity in modulating CCN activity across environments.

576 4. Conclusions

577 The mixing state of aerosol populations undergoes complex transformations
578 during atmospheric aging, altering the distribution of hygroscopic and non-hygroscopic
579 components and thus influencing CCN activity (Xu et al., 2021a; Ching et al., 2017).
580 This study derived a mixing state index (χ) from field-measured hygroscopicity
581 ~~probability density functions distributions~~, systematically investigating its impacts on
582 CCN activity ~~in at two~~ inland and coastal environments. Results provide field evidence
583 that aerosol mixing states generally reside between purely internal and external
584 extremes (Chen et al., 2022), ~~highlighting a dual regulatory mechanism of mixing state~~
585 ~~on CCN activity.~~ 2022b). Aerosol mixing state is largely influenced by the primary
586 emissions and secondary formation process. Externally-mixed particles with more
587 hydrophobic-mode originate chiefly from primary emissions in IAP, while that of more
588 sea-salt mode from sea spray in MHD. While it becomes more internally-mixed as the
589 enhanced fraction of more-hygroscopic mode and decreased of hydrophobic mode
590 during the aging process. This highlights a dual regulatory mechanism of mixing state
591 and its potential impact on hygroscopic distribution and CCN activity.

592 As χ increases, CN number concentrations (N_{CN}) first rise—driven by primary
593 emissions and new particle formation—then decline due to condensation and
594 coagulation during aging. Additionally, a logarithmic decreasing relationship between
595 critical diameter (D_{cri}) and χ was identified for both inland and coastal particles,
596 parameterized as $D_{\text{cri}} = -32.15\ln(\chi) + 84.71$ (Pearson $R = -0.74$, $R^2 = 0.54$). This offers
597 a practical approach to estimate D_{cri} from χ , serving as a general framework for

598 integrating mixing state effects on CCN activity in atmospheric models.

599 Entropy-based analyses confirm the pivotal role of mixing state in regulating N_{CCN} ,
600 especially for externally mixed aerosols: a 0.1 χ increase can enhance N_{CCN} by 39–65%.
601 Current models often oversimplify aerosol mixing states as purely internal or external
602 (Stevens et al., 2019; Bauer et al., 2013), the latter being particularly sensitive to organic
603 matter (Ren et al., 2018; Bhattu et al., 2015). Such simplifications introduce significant
604 biases in N_{CCN} estimation (Riemer et al., 2019; Ching et al., 2019). The χ - D_{crit}
605 parameterization proposed here offers a novel approach to reduce model complexity in
606 representing aerosol hygroscopicity and CCN activation, enabling more accurate
607 simulations of aerosol CCN capacity. It is expected mitigate the underestimation in
608 CCN compared with the complete external mixing assumption, while effectively
609 alleviates the overestimation that arises from applying the complete internal mixing
610 assumption in regions characterized by high external mixing (Zheng et al., 2021a). This
611 advancement improves our understanding of aerosol-cloud interactions (IPCC, 2021;
612 Rosenfeld et al., 2019), critical for refining climate effect assessments.

613 **Data availability**

614 All data used in the study are available at <https://doi.org/10.3974/geodb.2019.06.11.V1>
615 (Fan et al., 2019) and <http://doi.org/10.17632/3dx6pnx869.1> (Xu et al., 2021a).

616 **Author contributions**

617 RH and JR conceived the conceptual development of the paper. JR, FZ and WX directed
618 and performed the experiments with YW and LC. FZ and YS provided the dataset in

619 the inland site. JO, DC and CO provided the dataset in the coastal site. JR conducted
620 the data analysis and wrote the draft. All authors edited and commented on the various
621 sections of the paper.

622 **Competing interests**

623 The contact author has declared that none of the authors has any competing interests.

624 **Supporting Information**

625 Additional analysis results that were applied in this study. ~~Sensitivity~~Mean values
626 of the κ -PDF for aerosols of five diameters (Figure S1), sensitivity of the hygroscopic
627 parameter for the group of the hygroscopic species on the mixing state index χ (Figure
628 ~~S1), mean values of the κ -PDF for aerosols of five diameters (Figure S2),~~ time series
629 of the average per-particle species diversity $D\alpha$, the bulk population species diversity
630 $D\gamma$, and their affine ratio χ (Figure S3), diurnal trend of particle size, chemical mass
631 fraction and number fraction (NF) of hydrophobic and hygroscopic mode in IAP
632 (Figure S4) and in MHD (Figure S5), mixing state as a function of number fraction of
633 hydrophobic and hygroscopic mode (Figure S6), variation of the peak diameter (D_{peak})
634 with the mixing state index (Figure ~~S4~~S7), particle number size distribution and mixing
635 state during new particle formation events (Figure S8), diurnal variation of χ and CN
636 concentration during winter and summer periods for 40 nm and 150 nm aerosols in
637 inland and for 35 nm and 165 nm aerosols in coastal site (Figure ~~S5~~S9), relative change
638 of the critical diameter and CN concentration with the mixing state index χ (Figure
639 ~~S6~~S10) (PDF).

640 **Acknowledgements**

641 This work was funded by the National Natural Science Foundation of China (NSFC)
642 under Grant No. 42525301, 42405118 and 42475112, the State Key Laboratory of
643 Loess Science, Institute of Earth Environment, Chinese Academy of Sciences
644 (SKLLQG2429), the Guangdong Natural Science Foundation (Grant No.
645 2024A1515011005). We thank all participants of the field campaign for their hard work
646 and sharing of the data.

647 **References**

- 648 Bhattu, D., Tripathi, S. N.: CCN closure study: Effects of aerosol chemical composition
649 and mixing state, *Journal of Geophysical Research: Atmospheres.*, 120(2), 766–
650 783, <https://doi.org/10.1002/2014JD021978>, 2015.
- 651 Bellouin, N., Quaas, J., Gryspeerdt, E., Kinne, S., Stier, P., Watson-Parris, D., Boucher,
652 O., Carslaw, K. S., Christensen, M., Daniau, A.-L., Dufresne, J.-L., Feingold, G.,
653 Fiedler, S., ~~Forster~~Foster, P., Gettelman, A., Haywood, J. M., Lohmann, U.,
654 Malavelle, F., Mauritsen, T., McCoy, D. T., ~~Myhre, G., Mülmenstädt, J., Neubauer,~~
655 ~~D., Possner, A., Rugenstein, M., Sato, Y.~~Schulz, M., Schwartz, S. E., Sourdeval,
656 O., Storelvmo, T., Toll, V., Winker, D., ~~and~~Stevens, B.: Bounding global aerosol
657 radiative forcing of climate change, *Rev. Geophys.*, 58, e2019RG000660,
658 ~~<https://doi.org/>, 2019.~~<https://doi.org/10.1029/2019RG000660>, 2020.
- 659 Bauer, S. E., Ault, A., Prather, K. A.: Evaluation of aerosol mixing state classes in the
660 GISS modelE-MATRIX climate model using single-particle mass spectrometry
661 measurements, *Journal of Geophysical Research: Atmospheres.*, 118, 9834–9844,
662 <https://doi.org/10.1002/jgrd.50700>, 2013.
- 663 [Charlson, R. J., Schwartz, S. E., Hales, J. M., Cess, R. D., Coakley Jr, J. A., Hansen, J.](#)
664 [E., Hofmann, D. J.: Climate forcing by anthropogenic aerosols, *Science.*,](#)
665 [255\(5043\), 423–430, https://doi.org/10.1126/science.255.5043.423, 1992.](#)

666 Chen, Y., Haywood, J., Wang, Y., Malavelle, F., Jordan, G., Partridge, D., Fieldsend, J.,
667 Leeuw, J. D., Schmidt, A., Cho, N., Oreopoulos, L., Platnick, S., Grosvenor, D.,
668 Field, P., Lohmann, U.: Machine learning reveals climate forcing from aerosols is
669 dominated by increased cloud cover, *Nature Geoscience.*, 15(8), 609–614,
670 <https://doi.org/10.1038/s41561-022-01027-9>, ~~2022~~2022a.

671 ~~Chen, A., Zhao, C., Zhang, H., Yang, Y., Li, J.: Surface albedo regulates aerosol direct~~
672 ~~climate effect, *Nature Communications.*, 15(1), 7816, [https://doi.org/](https://doi.org/10.1038/s41467-024-52255-z)~~
673 ~~10.1038/s41467-024-52255-z, 2024.~~

674 ~~Chen, L., Zhang, F., Zhang, D., Wang, X., Song, W., Liu, J., Ren, J., Jiang, S., Li, X.,~~
675 ~~and Li, Z.: Measurement report: Hygroscopic growth of ambient fine particles~~
676 ~~measured at five sites in China, *Atmospheric Chemistry and Physics.*, 22, 6773-~~
677 ~~6786, <https://doi.org/10.5194/acp-22-6773-2022>, 2022b.~~

678 ~~Charlson, R. J., Schwartz, S. E., Hales, J. M., Cess, R. D., Coakley Jr, J. A., Hansen, J.~~
679 ~~E., Hofmann, D. J.: Climate forcing by anthropogenic aerosols, *Science.*,~~
680 ~~255(5043), 423–430, <https://doi.org/10.1126/science.255.5043.423>, 1992.~~

681 Ching, J., Zaveri, R. A., Easter, R. C., Riemer, N., Fast, J. D.: A three-dimensional
682 sectional representation of aerosol mixing state for simulating optical properties
683 and cloud condensation nuclei, *Journal of Geophysical Research: Atmospheres.*,
684 121(10), 5912–5929, <https://doi.org/10.1002/2015JD024323>, 2016.

685 ~~Ching, J., Fast, J., West, M., Riemer, N.: Metrics to quantify the importance of mixing~~
686 ~~state for CCN activity, *Atmospheric Chemistry and Physics.*, 17(12), 7445–7458,~~
687 ~~<https://doi.org/10.5194/acp-17-7445-2017>, 2017.~~

688 ~~Ching, J., Adachi, K., Zaizen, Y., Igarashi, Y., Kajino, M.: Aerosol mixing state revealed~~
689 ~~by transmission electron microscopy pertaining to cloud formation and human~~
690 ~~airway deposition, *npj Climate and Atmospheric Science.*, 2(1), 22, [https://doi.org/](https://doi.org/10.1038/s41612-019-0081-9)~~
691 ~~10.1038/s41612-019-0081-9, 2019.~~

692 Collins, D. B., Ault, A. P., Moffet, R. C., Ruppel, M. J., Cuadra-Rodriguez, L. A.,
693 Guasco, T. L., Corrigan, C. E., Pedler, B. E., Azam, F., Aluwihare, L. I., Bertram,
694 T. H., Roberts, G. C., Grassian, V. H., Prather, K. A.: Impact of marine

695 biogeochemistry on the chemical mixing state and cloud forming ability of nascent
696 sea spray aerosol, *Journal of Geophysical Research: Atmospheres.*, 118(15), 8553-
697 ~~8565~~, <https://doi.org/10.1002/jgrd.50598>, 2013.

698 Cheung, H. C., Chou, C. C. K., Lee, C. S. L., Kuo, W. C., Chang, S. C.: Hygroscopic
699 properties and cloud condensation nuclei activity of atmospheric aerosols under
700 the influences of Asian continental outflow and new particle formation at a coastal
701 site in eastern Asia, *Atmospheric Chemistry and Physics.*, 20(10), 5911–5922,
702 <https://doi.org/10.5194/acp-20-5911-2020>, 2020.

703 ~~Chen, L., Zhang, F., Zhang, D., Wang, X., Song, W., Liu, J., Ren, J., Jiang, S., Li, X.,
704 and Li, Z.: Measurement report: Hygroscopic growth of ambient fine particles
705 measured at five sites in China, *Atmospheric Chemistry and Physics.*, 22, 6773-
706 6786, <https://doi.org/10.5194/acp-22-6773-2022>, 2022.~~

707 Cai, J., Chu, B., Yao, L., Yan, C., Heikkinen, L. M., Zheng, F., Li, C., Fan, X., Zhang,
708 S., Yang, D., Wang, Y., Kokkonen, T. V., Chan, T., Zhou, Y., Dada, L., Liu, Y., He,
709 H., Paasonen, P., Kujansuu, J. T., Petäjä, T., Mohr, C., Kangasluoma, J., Bianchi,
710 F., Sun, Y., Croteau, P. L., Worsnop, D. R., Kerminen, V. M., Du, W., Kulmala, M.,
711 & Daellenbach, K. R.: Size-segregated particle number and mass concentrations
712 from different emission sources in urban Beijing, *Atmospheric Chemistry and
713 Physics.*, 20(21), 12721–12740, <https://doi.org/10.5194/acp-20-12721-2020>,
714 2020.

715 ~~Cai, M., Tan, H., Chan, C. K., Qin, Y., Xu, H., Li, F., Schurman, M, Dusek, U., Frank,
716 G. P., Hildebrandt, I., Liu, L., Zhao, Curtius, J.: The size resolved., Schneider, J.,
717 Walter, S., Chand, D., Drewnick, F., Hings, S., Jung, D., Borrmann, S., Andreae,
718 M. O.: Size matters more than chemistry for cloud condensation nuclei (CCN)
719 activity and its prediction based on nucleating ability of aerosol hygroscopicity
720 and composition in the Pearl Delta River (PRD) region during wintertime 2014,
721 *Atmospheric Chemistry and Physics.*, 18(22), 16419-16437,
722 <https://doi.org/10.5194/acp-18-16419-2018>, 2018.~~

723 ~~Ching, J., Fast, J., West, M., Riemer, N.: Metrics to quantify the importance of mixing~~

724 ~~state for CCN activity, Atmospheric Chemistry and Physics., 17(12), 7445-~~
725 ~~7458particles, Science., 312 (5778), 1375–1378, [https://doi.org/10.5194/acp-17-](https://doi.org/10.5194/acp-17-7445-2017)~~
726 ~~7445-2017, 20171126/science.1125261, 2006.~~

727 ~~Ching, J., Adachi, K., Zaizen, Y., Igarashi, Y., Kajino, M.: Aerosol mixing state revealed~~
728 ~~by transmission electron microscopy pertaining to cloud formation and human~~
729 ~~airway deposition, npj Climate and Atmospheric Science., 2(1), 22, [https://doi.org/](https://doi.org/10.1038/s41612-019-0081-9)~~
730 ~~10.1038/s41612-019-0081-9, 2019.~~

731 DeCarlo, P. F., Kimmel, J. R., Trimborn, A., Northway, M. J., Jayne, J. T., Aiken, A. C.,
732 Gonin, M., Fuhrer, K., Horvath, T., Docherty, K. S., Worsnop, D. R., Jimenez, J.
733 L.: Field-deployable, high-resolution, time of-flight aerosol mass spectrometer,
734 Analytical Chemistry., 78, 8281–8289, <https://doi.org/10.1021/ac061249n>, 2006.

735 Ervens, B., Cubison, M. J., Andrews, E., Feingold, G., Ogren, J. A., Jimenez, J. L.,
736 Quinn, P. K., Bates, T. S., Wang, J., Zhang, Q., Coe, H., Flynn, M., Allan, J. D.:
737 CCN predictions using simplified assumptions of organic aerosol composition and
738 mixing state: a synthesis from six different locations, Atmospheric Chemistry and
739 Physics., 10(10), 4795–4807, <https://doi.org/10.5194/acp-10-4795-2010>, 2010.

740 ~~Fierce, L., Onasch, T. B., Cappa, C. D., Mazzoleni, C., China, S., Bhandari, J.,~~
741 ~~Davidovits, P., Fischer, D. A., Helgestad, T., Lambe, A. T., et al.: Radiative~~
742 ~~absorption enhancements by black carbon controlled by particle-to-particle~~
743 ~~heterogeneity in composition, P. Natl. Acad. Sci. USA, 117, 5196–5203,~~
744 ~~<https://doi.org/10.1073/pnas.1919723117>, 2020.~~

745 Fan, X., Liu, J., Zhang, F., Chen, L., Collins, D., Xu, W., Jin, X., Ren, J., Wang, Y., Wu,
746 H., Li, S., Sun, Y., Li, Z.: Contrasting size-resolved hygroscopicity of fine particles
747 derived by HTDMA and HR-ToF-AMS measurements between summer and
748 winter in Beijing: the impacts of aerosol aging and local emissions, Atmospheric
749 Chemistry and Physics., 20(2), 915–929, [https://doi.org/10.5194/acp-20-915-](https://doi.org/10.5194/acp-20-915-2020)
750 ~~2020, 2020.~~

751 ~~Gong, X., Zhang, J., Croft, B., Yang, X., Frey, M. M., Bergner, N., Chang, R. Y. W.,~~
752 ~~Creamean, J. M., Kuang, C., Martin, R. V., Ranjithkumar, A., Sedlacek, A. J., Uin,~~

753 ~~J., Willmes, S., Zawadowicz, M. A., Pierce, J. R., Shupe, M. D., Schmale, J., Wang,~~
754 ~~J.: Arctic warming by abundant fine sea salt aerosols from blowing snow, Nature~~
755 ~~Geoscience., 16(9), 768–774, <https://doi.org/10.1038/s41561-023-01254-8>, 2023.~~
756 Gysel, M., Mcfiggans, G. B., Coe, H.: Inversion of tandem differential mobility
757 analyser (TDMA) measurements, *Journal of Aerosol Science.*, 40(2), 134–151,
758 <https://doi.org/10.1016/j.jaerosci.2008.07.013>, 2009.

759 Hughes, M., Kodros, J. K., Pierce, J. R., West, M., Riemer, N.: Machine learning to
760 predict the global distribution of aerosol mixing state metrics, *Atmosphere.*, 9(1),
761 15, <https://doi.org/10.3390/atmos9010015>, 2018.

762 Huang, R. J., Zhang, Y., Bozzetti, C., Ho, K. F., Cao, J. J., Han, Y., Daellenbach, K. R.,
763 Slowik, J. G., Platt, S. M., Canonaco, F., Zotter, P., Wolf, R., Pieber, S. M., Bruns,
764 E. A., Crippa, M., Ciarelli, G., Piazzalunga, A., Schwikowski, M., Abbaszade, G.,
765 Schnelle-Kreis, J., Zimmermann, R., An, Z., Szidat, S., Baltensperger, U., Haddad,
766 I. E., Prévôt, A. S.: High secondary aerosol contribution to particulate pollution
767 during haze events in China, *Nature.*, 514(7521), 218–222, [https://doi.org/](https://doi.org/10.1038/nature13774)
768 [10.1038/nature13774](https://doi.org/10.1038/nature13774), 2014.

769 IPCC. Summary for Policymakers. In *Climate Change 2021: The Physical Science*
770 *Basis. Contribution of Working Group I to the Sixth Assessment Report of the*
771 *Intergovernmental Panel on Climate Change*; Cambridge University Press:
772 Cambridge, United Kingdom and New York, NY, USA, 2021.

773 ~~Jimenez, J. L., Canagaratna, M. R., Donahue, N. M., Prevot, A. S. H., Zhang, Q., Kroll,~~
774 ~~J. H., DeCarlo, P. F., Allan, J. D., Coe, H., Ng, N. L., Aiken, A. C., Docherty, K.~~
775 ~~S., Ulbrich, I. M., Grieshop, A. P., Robinson, A. L., Duplissy, J., Smith, J. D.,~~
776 ~~Wilson, K. R., Lanz, V. A., Hueglin, C., Sun, Y., Tian, J., Laaksonen, A.,~~
777 ~~Raatikainen, T., Rautiainen, J., Vaattovaara, P., Ehn, M., Kulmala, M., Tomlinson,~~
778 ~~J. M., Collins, D. R., Cubison, M. J., Dunlea, E. J., Huffman, J. A., Onasch, T. B.,~~
779 ~~Alfarra, M. R., Williams, P. I., Bower, K., Kondo, Y., Schneider, J., Drewnick, F.,~~
780 ~~Bormann, S., Weimer, S., Demerjian, K., Salcedo, D., Cottrell, L., Griffin, R.,~~
781 ~~Takami, A., Miyoshi, T., Hatakeyama, S., Shimono, A., Sun, J., Zhang, Y., Dzepina,~~

782 ~~K., Kimmel, J. R., Sueper, D., Jayne, J. T., Herndon, S. C., Trimborn, A. M.,~~
783 ~~Williams, L. R., Wood, E. C., Middlebrook, A. M., Kolb, C. E., Baltensperger, U.,~~
784 ~~Worsnop, D. R.: Evolution of organic aerosols in the atmosphere, Science.,~~
785 ~~326(5959), 1525–1529, <https://doi.org/10.1126/science.1180353>, 2009.~~

786 ~~Liu, J., Zhang, F., Ren, J., Chen, L., Zhang, A., Wang, Z., Zou, S., Xu, H., Yue, X.: The~~
787 ~~evolution of aerosol mixing state derived from a field campaign in Beijing:~~
788 ~~implications for particle aging timescales in urban atmospheres, Atmospheric~~
789 ~~Chemistry and Physics., 25(9), 5075–5086, [https://doi.org/10.5194/acp-25-5075-](https://doi.org/10.5194/acp-25-5075-2025)~~
790 ~~2025, 2025.~~

791 Liu, P., Song, M., Zhao, T., Gunthe, S. S., Ham, S., He, Y., Qin, Y., Gong, Z., Amorim,
792 C. J., Bertram, K. A., Martin, S. T.: Resolving the mechanisms of hygroscopic
793 growth and cloud condensation nuclei activity for organic particulate matter,
794 Nature communications., 9(1), 4076, [https://doi.org/10.1038/s41467-018-06622-](https://doi.org/10.1038/s41467-018-06622-2)
795 2, 2018.

796 Liu, J., Zhang, F., Ren, J., Chen, L., Zhang, A., Wang, Z., Zou, S., Xu, H., Yue, X.: The
797 evolution of aerosol mixing state derived from a field campaign in Beijing:
798 implications for particle aging timescales in urban atmospheres, Atmospheric
799 Chemistry and Physics., 25(9), 5075–5086, [https://doi.org/10.5194/acp-25-5075-](https://doi.org/10.5194/acp-25-5075-2025)
800 2025, 2025.

801 Liu, Y., Lin, T., Zhang, J., Wang, F., Huang, Y., Wu, X., Ye, H., Zhang, G., Cao, X., and
802 de Leeuw, G.: Opposite effects of aerosols and meteorological parameters on
803 warm clouds in two contrasting regions over eastern China, Atmospheric
804 Chemistry and Physics., 24, 4651–4673, [https://doi.org/10.5194/acp-24-4651-](https://doi.org/10.5194/acp-24-4651-2024)
805 2024, 2024.

806 Lance, S., Nenes, A., Medina, J., Smith, J. N.: Mapping the operation of the DMT
807 continuous flow CCN counter, Aerosol Science and Technology., 40(4), 242–254,
808 <https://doi.org/10.1080/02786820500543290>, 2006.

809 Manavi, S. E. I., Aktypis, A., Siouti, E., Skyllakou, K., Myriokefalitakis, S., Kanakidou,
810 M., Pandis, S. N.: Atmospheric aerosol spatial variability: Impacts on air quality

811 and climate change, *One Earth.*, 8(3),
812 <https://doi.org/10.1016/j.oneear.2025.101237>, 2025.

813 Ovadnevaite, J., Ceburnis, D., Leinert, S., Dall'Osto, M., Canagaratna, M., O'Doherty,
814 S., Berresheim, H., O'Dowd, C.: Submicron NE Atlantic marine aerosol chemical
815 composition and abundance: Seasonal trends and air mass categorization, *Journal*
816 *of Geophysical Research: Atmospheres.*, 119, 11850–11863,
817 <https://doi.org/10.1002/2013JD021330>, 2014.

818 ~~Pan, Z., Mao, F., Rosenfeld, D., Zhu, Y., Zang, L., Lu, X., Thornton, J. A., Holzworth,~~
819 ~~R. H., Yin, J., Efrain, A., Gong, W.: Coarse Sea spray inhibits lightning, *Nature*~~
820 ~~*Communications.*, 13(1), 4289, <https://doi.org/10.1038/s41467-022-31714-5>,~~
821 ~~2022.~~

822 Petters, M. D., Kreidenweis, S. M.: A single parameter representation of hygroscopic
823 growth and cloud condensation nucleus activity, *Atmospheric Chemistry and*
824 *Physics.*, 7(8), 1961–1971, <https://doi.org/10.5194/acp-7-1961-2007>, 2007.

825 Padró, L. T., Moore, R. H., Zhang, X., Rastogi, N., Weber, R. J., and Nenes, A.: Mixing
826 state and compositional effects on CCN activity and droplet growth kinetics of
827 size-resolved CCN in an urban environment, *Atmospheric Chemistry and Physics.*,
828 2012, 12, 10239–10255, <https://doi.org/10.5194/acp-12-10239-2012>, 2012.

829 ~~Perkins, R. J., Marinescu, P. J., Levin, E. J. T., Collins, D. R., Kreidenweis, S. M.: Long-~~
830 ~~and short term temporal variability in cloud condensation nuclei spectra over a~~
831 ~~wide supersaturation range in the Southern Great Plains site, *Atmospheric*~~
832 ~~*Chemistry and Physics.*, 22(9), 6197–6215, [https://doi.org/10.5194/acp-22-6197-](https://doi.org/10.5194/acp-22-6197-2022)~~
833 ~~2022, 2022.~~

834 Rosenfeld, D., Zhu, Y., Wang, M., Zheng, Y., Goren, T., Yu, S.: Aerosol- driven droplet
835 concentrations dominate coverage and water of oceanic low-level clouds, *Science.*,
836 363(6427), <https://doi.org/10.1126/science.aay4194>, 2019.

837 Riemer, N., Ault, A. P., West, M., Craig, R. L., Curtis, J. H.: Aerosol mixing state:
838 Measurements, modeling, and impacts, *Reviews of Geophysics.*, 57(2), 187–249,
839 <https://doi.org/10.1029/2018RG000615>, 2019.

840 Ren, J., Zhang, F., Wang, Y., Collins, D., Fan, X., Jin, X., Xu, W., Sun, Y., Cribb, M.,
841 Li, Z.: Using different assumptions of aerosol mixing state and chemical
842 composition to predict CCN concentrations based on field measurements in urban
843 Beijing, *Atmospheric Chemistry and Physics.*, 18(9), 6907–6921,
844 <https://doi.org/10.5194/acp-18-6907-2018> 2018.

845 Ramachandran, S., Srivastava, R.: Mixing states of aerosols over four environmentally
846 distinct atmospheric regimes in Asia: coastal, urban, and industrial locations
847 influenced by dust, *Environmental Science and Pollution Research.*, 23, 11109–
848 11128, <https://doi.org/10.1007/s11356-016-6254-8>, 2016.

849 Ren, J., Zhang, F., Chen, L., Cao, G., Liu, M., Li, X., Wu, H., Cheng, Y., and Li, Z.:
850 Identifying the hygroscopic properties of fine aerosol particles from diverse
851 sources in urban atmosphere and the applicability in prediction of cloud nuclei,
852 *Atmos. Environ.*, 298, 119615, <https://doi.org/10.1016/j.atmosenv.2023.119615>,
853 2023.

854 Rierner, N. and West, M.: Quantifying aerosol mixing state with entropy and diversity
855 measures, *Atmospheric Chemistry and Physics.*, 13, 11423–11439,
856 <https://doi.org/10.5194/acp-13-11423-2013>, 2013.

857 Rose, D., Gunthe, S. S., Mikhailov, E., Frank, G. P., Dusek, U., Andreae, M. O., Pöschl,
858 U.: Calibration and measurement uncertainties of a continuous-flow cloud
859 condensation nuclei counter (DMT-CCNC): CCN activation of ammonium sulfate
860 and sodium chloride aerosol particles in theory and experiment, *Atmospheric*
861 *Chemistry and Physics.*, 8(5), 1153–1179, [https://doi.org/10.5194/acp-8-1153-](https://doi.org/10.5194/acp-8-1153-2008)
862 2008, 2008.

863 Shrivastava, M., Cappa, C. D., Fan, J., Goldstein, A. H., Guenther, A. B., Jimenez, J.
864 L., Kuang, C., Laskin, A., Martin, S. T., Ng, N. L., Petaja, T., Pierce, J. R., Rasch,
865 P. J., Roldin, P., Seinfeld, J. H., Shilling, J., Smith, J. N., Thornton, J. A., Volkamer,
866 R., Wang, J., Worsnop, D. R., Zaveri, R. A., Zelenyuk, A., Zhang, Q.: Recent
867 advances in understanding secondary organic aerosol: Implications for global
868 climate forcing, *Reviews of Geophysics.*, 55(2), 509–559,

869 <https://doi.org/10.1002/2016RG000540>, 2017.

870 Stevens, R., and Dastoor, A.: A Review of the Representation of Aerosol Mixing State
871 in Atmospheric Models, *Atmosphere.*, 10, 168,
872 <https://doi.org/10.3390/atmos10040168>, 2019.

873 [Spitieri, C., Gini, M., Gysel-Beer, M., and Eleftheriadis, K.: Annual cycle of](#)
874 [hygroscopic properties and mixing state of the suburban aerosol in Athens, Greece,](#)
875 [Atmospheric Chemistry and Physics.](#), 23, 235–249, [https://doi.org/10.5194/acp-](https://doi.org/10.5194/acp-23-235-2023)
876 [23-235-2023](#), 2023.

877 Sotiropoulou, R. E. P., Nenes, A., Adams, P. J., Seinfeld, J. H.: Cloud condensation
878 nuclei prediction error from application of Köhler theory: Importance for the
879 aerosol indirect effect, *Journal of Geophysical Research: Atmospheres.*, 112(D12),
880 <https://doi.org/10.1029/2006JD007834>, 2007.

881 Schill, S. R., Collins, D. B., Lee, C., Morris, H. S., Novak, G. A., Prather, K. A., Quinn,
882 P. K., Sultana, C. M., Tivanski, A. V., Zimmermann, K., Cappa, C. D., Bertram, T.
883 H.: The impact of aerosol particle mixing state on the hygroscopicity of sea spray
884 aerosol, *ACS central science.*, 1(3), 132-141,
885 <https://doi.org/10.1021/acscentsci.5b00174>, 2015.

886 [Shi, Z., Vu, T., Kotthaus, S., Harrison, R. M., Grimmond, S., Yue, S., Zhu, T., Lee, J.,](#)
887 [Han, Y., Demuzere, M., Dunmore, R. E., Ren, L., Liu, D., Wang, Y., Wild, O.,](#)
888 [Allan, J., Acton, W. J., Barlow, J., Barratt, B., Beddows, D., Bloss, W. J., Calzolari,](#)
889 [G., Carruthers, D., Carslaw, D. C., Chan, Q., Chatzidiakou, L., Chen, Y., Crilley,](#)
890 [L., Coe, H., Dai, T., Doherty, R., Duan, F., Fu, P., Ge, B., Ge, M., Guan, D.,](#)
891 [Hamilton, J. F., He, K., Heal, M., Heard, D., Hewitt, C. N., Hollaway, M., Hu, M.,](#)
892 [Ji, D., Jiang, X., Jones, R., Kalberer, M., Kelly, F. J., Kramer, L., Langford, B.,](#)
893 [Lin, C., Lewis, A. C., Li, J., Li, W., Liu, H., Liu, J., Loh, M., Lu, K., Lucarelli, F.,](#)
894 [Mann, G., McFiggans, G., Miller, M. R., Mills, G., Monk, P., Nemitz, E., O'Connor,](#)
895 [F., Ouyang, B., Palmer, P. I., Percival, C., Popoola, O., Reeves, C., Rickard, A. R.,](#)
896 [Shao, L., Shi, G., Spracklen, D., Stevenson, D., Sun, Y., Sun, Z., Tao, S., Tong, S.,](#)
897 [Wang, Q., Wang, W., Wang, X., Wang, X., Wang, Z., Wei, L., Whalley, L., Wu, X.,](#)

988 [Wu, Z., Xie, P., Yang, F., Zhang, Q., Zhang, Y., Zhang, Y., and Zheng, M.: Introduction to the special issue “In-depth study of air pollution sources and processes within Beijing and its surrounding region \(APHH-Beijing\)”, Atmospheric Chemistry and Physics., 19, 7519–7546, <https://doi.org/10.5194/acp-19-7519-2019>, 2019.](#)

989

990

991

992

993 Stokes, R. H., Robinson, R. A.: Interactions in aqueous nonelectrolyte solutions. I.

994 Solute-Solvent equilibria, *Journal of Physical Chemistry.*, 70(7), 2126–2130,

995 <https://doi.org/10.1021/j100879a010>, 1966.

996 [Tao, J., Kuang, Y., Ma, N., Hong, J., Sun, Y., Xu, W., Zhang, Y., He, Y., Luo, Q., Xie, L., Su, H., and Cheng, Y.: Secondary aerosol formation alters CCN activity in the North China Plain, Atmospheric Chemistry and Physics., 21, 7409–7427, <https://doi.org/10.5194/acp-21-7409-2021>, 2021.](#)

997

998

999

1000

1001 [Tao, J., Luo, B., Xu, W., Zhao, G., Xu, H., Xue, B., Zhai, M., Xu, W., Zhao, H., Ren, S., Zhou, G., Liu, L., Kuang, Y., and Sun, Y.: Markedly different impacts of primary emissions and secondary aerosol formation on aerosol mixing states revealed by simultaneous measurements of CCNC, H\(V\)TDMA, and SP2, Atmospheric Chemistry and Physics., 24, 9131–9154, <https://doi.org/10.5194/acp-24-9131-2024>, 2024.](#)

1002

1003

1004

1005

1006

1007

1008

1009

1010

1011

1012

1013

1014

1015

1016 Virtanen, A., Joutsensaari, J., Kokkola, H., Partridge, G. D., Blichner, S., Seland, Ø.,

1017 Holopainen, E., Tovazzi, E., Lipponen, A., Mikkonen, S., Leskinen, A., Hyvärinen,

1018 A., Zieger, P., Krejci, R., Ekman, A. M. L., Riipinen, I., Quaas, J., Romakkaniemi,

1019 S.: High sensitivity of cloud formation to aerosol changes, *Nature Geoscience.*, 1–

1020 =7, <https://doi.org/10.1038/s41561-025-01662-y>, 2025.

1021

1022

1023

1024

1025

1026 Winkler, P.: The growth of atmospheric aerosol particles as a function of the relative

humidity—II. An improved concept of mixed nuclei, *Journal of Aerosol Science.*,

4(5), 373–387, [https://doi.org/10.1016/0021-8502\(73\)90027-X](https://doi.org/10.1016/0021-8502(73)90027-X), 1973.

Wang, J., Cubison, M. J., Aiken, A. C., Jimenez, J. L., Collins, D. R.: The importance

of aerosol mixing state and size-resolved composition on CCN concentration and

the variation of the importance with atmospheric aging of aerosols, *Atmospheric*

927 Chemistry and Physics., 10(15), 7267–7283, <https://doi.org/10.5194/acp-10->
928 7267-2010, 2010.

929 Wang, Y., Li, Z., Zhang, R., Jin, X., Xu, W., Fan, X., et al.: Distinct ultrafine- and
930 accumulation-mode particle properties in clean and polluted urban environments,
931 Geophysical Research Letters., 46, 10,918–10,925,
932 <https://doi.org/10.1029/2019GL084047>, 2019.

933 Xu, W., Ovadnevaite, J., Fossum, K. N., Lin, C., Huang, R. J., Ceburnis, D., O’Dowd,
934 C.: Sea spray as an obscured source for marine cloud nuclei, Nature Geoscience.,
935 15(4), 282–286, <https://doi.org/10.1038/s41561-022-00917-2>, 2022.

936 Xu, W., Ovadnevaite, J., Fossum, K. N., Huang, R. J., Huang, D., Zhong, H., Gu, Y.,
937 Lin, C., Huang, C., O’Dowd, C., Ceburnis, D.: Condensation of organic-inorganic
938 vapours governs the production of ultrafine secondary marine cloud nuclei,
939 Communications Earth & Environment., 5(1), 359,
940 <https://doi.org/10.1038/s43247-024-01519-z>, 2024.

941 Xu, W., Ovadnevaite, J., Fossum, K. N., Lin, C., Huang, R. J., O’Dowd, C., Ceburnis,
942 D.: Aerosol hygroscopicity and its link to chemical composition in the coastal
943 atmosphere of Mace Head: marine and continental air masses, Atmospheric
944 Chemistry and Physics., 20(6), 3777–3791, <https://doi.org/10.5194/acp-20-3777->
945 2020, 2020.

946 Xu, W., Ovadnevaite, J., Fossum, K. N., Lin, C., Huang, R.-J., O’Dowd, C., Ceburnis,
947 D.: Seasonal trends of aerosol hygroscopicity and mixing state in clean marine and
948 polluted continental air masses over the Northeast Atlantic, Journal of Geophysical
949 Research: Atmospheres., 126, e2020JD033851,
950 <https://doi.org/10.1029/2020JD033851>, 2021a.

951 ~~Xu, W., Fossum, K. N., Ovadnevaite, J., Lin, C., Huang, R. J., O’Dowd, C., Ceburnis,~~
952 ~~D.: The impact of aerosol size dependent hygroscopicity and mixing state on the~~
953 ~~cloud condensation nuclei potential over the north east Atlantic, Atmospheric~~
954 ~~Chemistry and Physics., 21(11), 8655–8675, <https://doi.org/10.5194/acp-21-8655->~~
955 ~~2021, 2021b.~~

956 ~~Xu, W., Ovadnevaite, J., Fossun, K. N., Lin, C., Huang, R. J., O'Dowd, C., Ceburnis,~~
957 ~~D.: Aerosol hygroscopicity and its link to chemical composition in the coastal~~
958 ~~atmosphere of Mace Head: marine and continental air masses, Atmospheric~~
959 ~~Chemistry and Physics., 20(6), 3777-3791, [https://doi.org/10.5194/acp-20-3777-](https://doi.org/10.5194/acp-20-3777-2020)~~
960 ~~2020, 2020.~~

961 ~~Xu, W.,~~ Sun, Y., Wang, Q., Zhao, J., Wang, J., Ge, X., Xie, C., Zhou, W., Du, W., Li, J.,
962 Fu, P., Wang, Z., Worsnop, D. R., Coe, H.: Changes in aerosol chemistry from
963 2014 to 2016 in winter in Beijing: Insights from high-resolution aerosol mass
964 spectrometry, *Journal of Geophysical Research: Atmospheres.*, 124, 1132–1147,
965 <https://doi.org/10.1029/2018JD029245>, 2019.

966 ~~Xu, W., Ovadnevaite, J., Fossun, K. N., Lin, C., Huang, R. J., Ceburnis, D., O'Dowd,~~
967 ~~C.: Sea spray as an obscured source for marine cloud nuclei, Nature Geoscience.,~~
968 ~~15(4), 282-286, <https://doi.org/10.1038/s41561-022-00917-2>, 2022.~~

969 ~~Xu, W., Ovadnevaite, J., Fossun, K. N., Huang, R. J., Huang, D., Zhong, H., Gu, Y.,~~
970 ~~Lin, C., Huang, C., O'Dowd, C., Ceburnis, D.: Condensation of organic-inorganic~~
971 ~~vapours governs the production of ultrafine secondary marine cloud nuclei,~~
972 ~~Communications Earth & Environment., 5(1), 359,~~
973 ~~<https://doi.org/10.1038/s43247-024-01519-z>, 2024.~~

974 Xie, C., He, Y., Lei, L., Zhou, W., Liu, J., Wang, Q., Xu, W., Qiu, Y., Zhao, J., Sun, J.,
975 Li, L., Li, M., Zhou, Z., Fu, P., Wang, Z., Sun, Y.: Contrasting mixing state of black
976 carbon-containing particles in summer and winter in Beijing, *Environmental*
977 *Pollution.*, 263, 114455, <https://doi.org/10.1016/j.envpol.2020.114455>, 2020.

978 ~~Xu, W., Fossun, K. N., Ovadnevaite, J., Lin, C., Huang, R. J., O'Dowd, C., Ceburnis,~~
979 ~~D.: The impact of aerosol size-dependent hygroscopicity and mixing state on the~~
980 ~~cloud condensation nuclei potential over the north-east Atlantic, Atmospheric~~
981 ~~Chemistry and Physics., 21(11), 8655–8675, [https://doi.org/10.5194/acp-21-8655-](https://doi.org/10.5194/acp-21-8655-2021)~~
982 ~~2021, 2021b.~~

983 Ye, Q., Gu, P., Li, H. Z., Robinson, E. S., Lipsky, E. M., Kaltsonoudis, C., Lee, A. K.
984 Y., Apte, J. S., Robinson, A. L., Sullivan, R. C., Presto, A. A., Donahue, N. M.:

985 Spatial variability of sources and mixing state of atmospheric particles in a
986 metropolitan area, *Environmental Science & Technology.*, 52, 6807–6815,
987 <https://doi.org/10.1021/acs.est.8b01011>, 2018.

988 Yuan, L., and Zhao, C.: Quantifying particle-to-particle heterogeneity in aerosol
989 hygroscopicity, *Atmospheric Chemistry and Physics.*, 23, 3195–3205,
990 <https://doi.org/10.5194/acp-23-3195-2023>, 2023.

991 Yang, F., Chen, H., Du, J., Yang, X., Gao, S., Chen, J., Geng, F.: Evolution of the mixing
992 state of fine aerosols during haze events in Shanghai, *Atmospheric Research.*, 104:
993 193-201, <https://doi.org/10.1016/j.atmosres.2011.10.005>, 2012.

994 ~~Zheng, Z., West, M., Zhao, L., Ma, P.-L., Liu, X., and Riemer, N.: Quantifying the~~
995 ~~structural uncertainty of the aerosol mixing state representation in a modal model,~~
996 ~~*Atmospheric Chemistry and Physics.*, 21, 17727–17741,~~
997 ~~<https://doi.org/10.5194/acp-21-17727-2021>, 2021.~~

998 ~~Zheng, Z.,~~ Curtis, J. H., Yao, Y., Gasparik, J. T., Anantharaj, V. G., Zhao, L., West, M.,
999 Riemer, N.: Estimating submicron aerosol mixing state at the global scale with
1000 machine learning and Earth system modeling, *Earth and Space Science.*, 8(2),
1001 e2020EA001500, <https://doi.org/10.1029/2020EA001500>, ~~2021~~2021a.

1002 ~~Zheng, Z., West, M., Zhao, L., Ma, P.-L., Liu, X., and Riemer, N.: Quantifying the~~
1003 ~~structural uncertainty of the aerosol mixing state representation in a modal model,~~
1004 ~~*Atmospheric Chemistry and Physics.*, 21, 17727–17741,~~
1005 ~~<https://doi.org/10.5194/acp-21-17727-2021>, 2021b.~~

1006 ~~Zhao, G., Tan, T., Zhu, Y., Hu, M., and Zhao, C.: Method to quantify black carbon~~
1007 ~~aerosol light absorption enhancement with a mixing state index, *Atmospheric*~~
1008 ~~*Chemistry and Physics.*, 21, 18055–18063, <https://doi.org/10.5194/acp-21-18055->~~
1009 ~~2021, 2021.~~

1010 Zdanovskii, A.: New methods for calculating solubilities of electrolytes in
1011 multicomponent systems, *Zh. Fiz. Khim. C*, 22, 1475–1485, 1948.

1012 Zhong, H., Huang, R. J., Lin, C., Xu, W., Duan, J., Gu, Y., Huang, W., Ni, H.; Zhu, C.,
1013 You, Y., Wu, Y., Zhang, R., Ovadnevaite, J., Ceburnis, D., O'Dowd, C.:

1014 Measurement report: On the contribution of long-distance transport to the
1015 secondary aerosol formation and aging, *Atmospheric Chemistry and Physics.*, 22,
1016 9513–9524, <https://doi.org/10.5194/acp-22-9513-2022>, 2022.